Test method for measuring electrical resistivity of UD CFRP materials with off-axis fibre orientations

A study towards a better understanding of the electrical behaviour within the complex fibre network of UD CFRP's

Master thesis in Mechanical Engineering

A.A. Coulibaly
June 1, 2023

Chair of Production Technology,
Department of Mechanical Engineering,
Faculty of Engineering Technology,
University of Twente, Enschede

Exam committee
Chair: Dr.ir. T.C. Bor
Internal supervisor: Ir. Y.M. Buser
Internal supervisor: Dr.ir. W.J.B. Grouve
External member: Dr. M. Feinageule

Summary

Carbon fibre reinforced polymer composites (CFRPs) are showing increased promise in the aerospace industry due to their excellent mechanical properties and low density. Specifically thermoplastic composites are gaining interest because of their melt processability that provides advantages in terms of part manufacturing and assembly. Induction welding is one of the more attractive assembly technologies that utilizes the melt-processability of the thermoplastic matrix. The process utilizes an induction coil to generate eddy currents in the carbon fiber network which, as a result of their resistivity, will heat in order to melt the surrounding matrix material. Although the process is already used in practice, it still relies on time-consuming and expensive trial-and-error procedures to define processing windows. A numerical model capable of predicting the heat generation inside of a CFRP laminate during induction heating would provide significant value and reduce the costs and time associated with process development.

One of the challenges towards process simulation is predicting and characterizing the electrical behaviour of the bulk composite material. The aim of the present work is to design a comprehensive test method for measuring the flow of current inside unidirectional (UD) CFRP laminates along directions that are not parallel with the fibres. Numerical modelling is used to simulate, and visualize, electrical phenomena within the composite material with the aim to design the test setup. Six line-contact electrodes are used to run current through specimens, and simultaneously measure voltage differences at the top and bottom surfaces of said specimen. It is found that equipotential lines form parallel to the fibre orientation of UD laminates. Along these lines, the electric potential is constant. As a result of this, line-contact electrodes must be placed parallel to the fibre orientation to avoid short circuits that can influence measurement data. Based on the simulations, the test method is designed, developed, and subsequently employed to characterize three common materials used in the aerospace industry. Significant error is found between the measured values, and the values predicted using analytical expressions. This means that physical measurements are still necessary to determine the off-axis resistivity. Further research into the electrical behaviour of composite materials is necessary to reduce this error; and to ensure that models capable of accurately predicting directional resistivity regardless of fibre orientation can be built.

Contents

Chapter 1

Introduction

1.1 Background

The investment in research and development of new and existing materials and technologies is a continuous trend in any industry. Common goals include, but are not limited to: improving performance, improving sustainability, and reducing costs. Composite materials have been of much interest to the aerospace industry due to their high strength-to-weight ratio and outstanding fatigue resistance [1]. Composite aircraft parts often have a higher initial cost when compared to their metal counterparts. However, they can provide cost savings in the long term when considering fuel consumption and the fact that less maintenance is required. Fibre reinforced polymer composites are showing the most promise in the aerospace industry, out of the wide range of specialised composite materials available in the current market. These composites are built from multiple stacked plies. Where each ply consists of a reinforcing fibre material embedded inside a surrounding polymer matrix material.

Polymer composite materials can be classified in different ways. A classification by fiber length is most natural. Short and long fiber composites feature discontinuous fibers. These materials combine good performance with excellent processability. As an alternative, one can use continuous fibers. This type of reinforcement is typically more expensive, but can provide better performance in terms of higher: strength, stiffness, toughness, and fatigue resistance. In the case of the latter, the fibres can be arranged in weave patterns similar to textiles, also referred to as fabrics. The type of fibre reinforcement has a non-trivial impact on certain properties of the composite material. This work focuses on unidirectional (UD) continuous fibres, where all fibres within the same ply are arranged in the same general direction. The specific material of both the matrix and fibres have significant influence on the properties of the bulk composite material, similarly to the fibre reinforcement type.

Most commonly, fibres are made of strong and stiff materials. The majority of the fibres used by the aerospace industry are: carbon, glass, and aramid or kevlar [1, 3]. Out of the three, carbon is most commonly used as it provides a high tensile modulus, low weight, and good chemical stability. However, a case could be made for any of the presented fibre materials depending on the application. Figure 1.1 illustrates how the fibres are arranged in a UD ply. Additionally, the material coordinate system and its principal directions are defined in relation to the ply and to the global coordinate system. The z- and 3-direction are on the same axis. The xy-plane is thus coincident with the 12-plane. However there is an offset between the x- and 1-axis in the form of an angle θ which is defined as a rotation around the z-axis (or 3-axis). These principal directions are referred to throughout the remainder of this work.

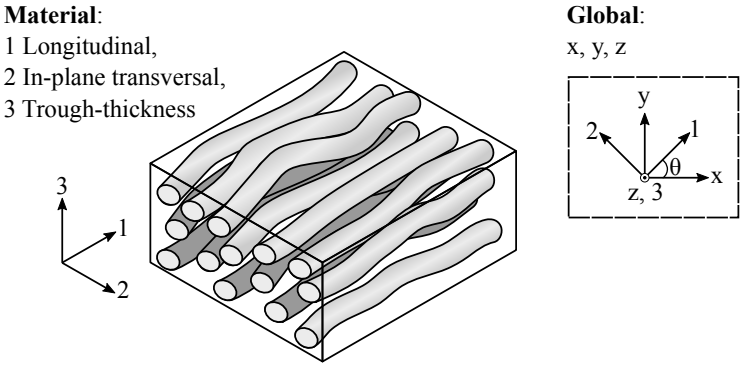

Figure 1.1: *Principal directions of a UD ply (material coordinate system) relative to the global coordinate system. Adapted from [2].*

Thermoplastics show a lot of promise, when it comes to polymeric matrix materials for aerospace applications. While thermosets have their merit in certain applications, the processing flexibility that thermoplastics provide is unrivaled. Thermoplastics can be molten, or softened, to be shaped and re-shaped multiple times in multi-step thermal processes. This allows for significantly more flexibility during the manufacturing of parts. Due to this, thermoplastic parts can also be recycled and repurposed for new, less demanding, applications; though the mechanical properties of the polymer do reduce each time. Furthermore, processing speeds for thermoplastics can often be much higher when compared to thermosets.

One of the operations where the manufacturing flexibility of thermoplastics is considered advantageous is the joining of parts during manufacturing of complex multi-component assemblies, such as airplanes. Themoplastic parts can be welded, whereas thermoset parts require joining through adhesion or mechanical fastening. Welding can create strong bonds with high speed and low manual labor in contrast to adhesion or mechanical fastening. The most mature welding technologies for joining thermoplastic parts are currently resistance welding, ultrasonic welding, and induction welding [4, 5]. Out of these, induction welding is showing a lot of promise due the ability to make long continuous welds without introducing any foreign material at the weld interface.

1.2 Problem statement

Welding of carbon fibre reinforced thermoplastic composites (CFRP) through electromagnetic induction enables rapid assembly of complex structures. Additionally, potential critical points for failure are diminished by there being no foreign material at the interface and no need for drilling or punching holes in the parts. Parts are fused into a single, homogeneous, part. Induction welding simultaneously takes advantage of the re-meltability of thermoplastics and the electrical conductivity of carbon fibres to create a satisfactory bond. The weld interface is heated by means of induction. Concurrently, pressure is applied at the interface to facilitate the fusion process; which serves to consolidate the joint interface. Additionally, when a composite part is heated past the melting point of the matrix material, de-consolidation can occur between the separate layers of the composite. Therefore, the applied welding pressure not only ensure a strong bond at the weld interface, free of air voids, but also does this for all other interfaces between the individual layers of the composite parts. The desired weld can then be achieved by moving the coil along the weld line. The most important process parameters are: the strength of the magnetic field, the displacement rate of the coil over the material, and the applied pressure at the weld interface. While the effect that these process

parameters have on the achieved temperature at the weld ling is generally understood, finding appropriate processing windows still largely relies on trial and error.

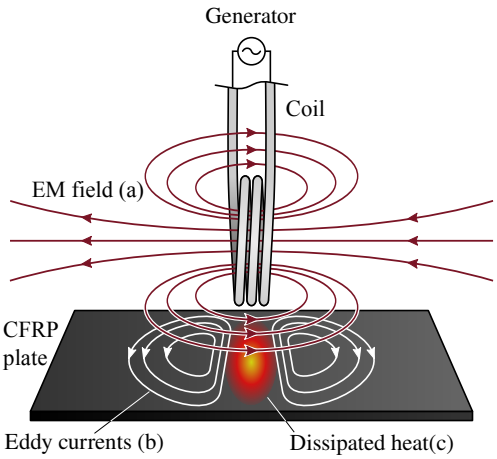

Figure 1.2: *Induction heating of CFRP plate. Taken from [2].*

To further increase the viability of induction welding as a competitive joining process in the aerospace industry, the process of induction heating for CFRP's must first be fully understood. Figure 1.2 visualizes the steps involved. Induction heating occurs when exposing the composite parts to an alternating electromagnetic field, that is generated by an alternating current in a conductive, air-core, coil (Figure 1.2 (a)). The magnetic field generates eddy currents in the network of electrically conductive carbon fibres within the composite parts (Figure 1.2 (b)). The electrical resistance of the fibres causes energy to be lost as heat, which is dissipated to the surrounding thermoplastic matrix (Figure 1.2 (c)). This causes the thermoplastic to soften or melt, allowing for the material to be further processed.

During induction heating of CFRP's, there are three heating mechanisms that can contribute to the overall heating. All three are a form of resistance heating, with the difference being the element providing the electrical resistance. Fibre heating is caused by the resistance of the fibre itself. While contact heating is caused by the resistance of the contact interface between fibres. Dielectric hysteresis is a result of the capacitor effect generated by a potential difference between fibres separated by a thin layer of matrix material. This is most common at the bond interface between adjacent plies, where the matrix material acts as a dielectric. Figure 1.3 shows an example case for a UD cross-ply laminate with a [90/0] layup. The current can both flow along the fibres, and through fibre contacts. Because of this, the manner in which the fibres are organized has an impact on the relative contribution of the different heating mechanisms outlined in Figure 1.3. It must be noted that dielectric hysteresis does not occur with direct currents (DC); it can only occur with alternating currents (AC) operating in the kilohertz (kHz) to megahertz (MHz) range. [6–12]

A numerical model capable of predicting the electromagnetic heating inside of a CFRP laminate during induction heating would provide significant value for a process such as induction welding. Currently, trial and error is still largely necessary to achieve good welds through induction. The repeatability of the welds must be improved to eliminate this. Increasing the repeatability demands high predictability of the temperature profile within the part. There are, however, still challenges regarding the implementation of a model capable of accurately predicting this temperature profile. One of these challenges is simulating the electrical behaviour of the complex carbon fibre network inside the polymer matrix. In the case of UD CFRP's, the

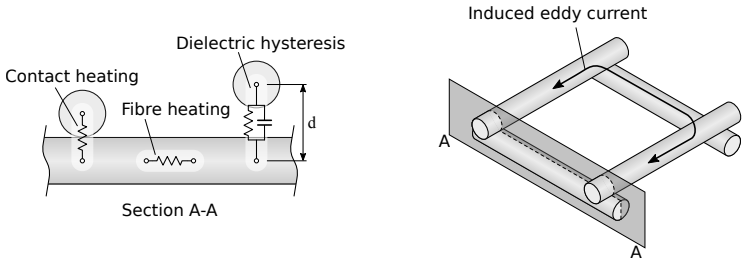

Figure 1.3: *Relevant heating mechanisms during induction heating of CFRP's. Taken from [2].*

fibre orientation in the plies is critical in determining electrical properties of the the bulk laminate. This can ultimately affect the heating experienced by the material. Being able to predict how fibre orientation affects electrical conductivity is thus a crucial step towards a full induction model for UD CFRP's. In time, such a model would be able to simulate the effect of a generated electromagnetic field on any weld geometry and material combination. The foremost condition for this to be possible, is to build a model which is accurate enough. This accuracy can be validated through experimental methods.

1.3 Objective & approach

This work is meant as a contribution to the ongoing research on induction heating of composites. The objective is to develop, and outline, a reliable test method for measuring the electrical resistivity of UD CFRP laminates with off-axis fibre orientations. In the context of this work, off-axis directions are any direction in the xy-plane, non-parallel to the x- or y-axes. Namely, this holds for $0^\circ < \theta < 90^\circ$ (see Fig. 1.1). Literature regarding electrical measurements of UD CFRP materials is reviewed to give an overview of commonly employed methods. This is also used as a foundation for the test method described in this work. Numerical modeling is used to explore, and visualize, certain electrical phenomena that can influence measurements. This is done using COMSOL Multiphysics. The insights gained regarding the electrical behaviour of anisotropic materials, such as UD CFRP's, are used as guidelines to design an appropriate test method. The method is then applied to investigate three highly relevant materials in the current aerospace industry: C/PEEK, C/PEKK, and C/LMPAEK.

The results obtained through the measurement method can be used to determine whether the directional electrical resistivity of a UD laminate can be predicted using analytical expressions; regardless of fibre orientation. The versatile test method presented in this work is a step towards better understanding of the electrical behaviour inside the complex fibre networks of UD CFRP materials. Which, in time, can be used to build an accurate induction heating model for UD CFRP materials.

Chapter 2

Theory & Literature

In this chapter, essential concepts and properties related to the electrical behavior of UD CFRP materials are put forth. This serves as a foundation for the work presented in subsequent chapters. First, the fundamentals of electrical resistivity are explained, together with its relation to electrical conductivity. This understanding is then used to explain how one could measure these properties. Analytical expressions are proposed, relating the electrical resistivity to measurable parameters. Furthermore, current literature is reviewed to compare experimental results and reveal important measuring considerations. From this, it is found that the behaviour of equipotentials, inside UD CFRP materials, could be a crucial consideration often neglected by literature.

2.1 Electrical resistivity and conductivity

The electrical resistivity, sometimes referred to as volume resistivity, is an intrinsic property that signifies the ability of a material to resist the flow of electric current. A material with lower resistivity allows for easier passage of current. In this work, resistivity is denoted by ρ, and is given in its SI units of $[\Omega m]$:

$$\rho = \frac{RA}{\delta} \tag{2.1}$$

where R $[\Omega]$ is the electrical resistance of the material, δ [m] is the length of the material, and A $[\mathrm{m}^2]$ is the cross-sectional area of the material normal to the direction in which δ is defined. Figure 2.1 illustrates how these characteristics relate to the material. One can imagine the resistive material as a wire with electrical contacts on each end. At first glance it seems that the resistivity decreases as the wire increases in length. However, this is not the case. A way to interpret this is that the wire is part of a closed loop electrical circuit. The resistance (R) is a variable which depends on the geometry of the wire in this case. As the wire increases in length, the resistance of this circuit grows proportionally. Therefore, the resistivity (ρ) is independent of the form or length of the wire.

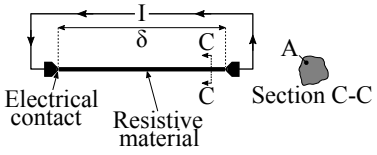

Figure 2.1: *A material of arbitrary volume ($\delta \times A$) subjected to an electric current (I).*

On the other hand, the electrical conductivity signifies the ability of a material to conduct electric current,

and is defined as the reciprocal of resistivity. In this work conductivity is denoted by σ, and is given in its SI units of [S/m]. The simple relation between ρ and σ implies that they can be used interchangeably. However, one must be careful with the usage of this relation when it comes to CFRP materials.

Resistivity and conductivity are in fact directional properties. This means that the resistivity or conductivity of a material take the form of a second order tensor (see Equations 2.2 and 2.3). In its basic form, the off-diagonal terms are zero, and the diagonal terms represent the property in the given principal directions. For isotropic materials, such as metals, this tensor can be reduced to a single value. This is because all diagonal terms are equal to each other; in other words, the resistivity or conductivity is the same in all directions inside the material. However, for anisotropic materials, such as CFRP's, the diagonal terms take on different values. The simple relation between ρ and σ holds for isotropic materials. In the case of anisotropic materials, a similar, but crucially distinct, relation holds: the conductivity in a principal direction is the reciprocal of the resistivity in the same principal direction. For example: $\rho_1 = 1/\sigma_1$.

In the context of this work, it is useful to consider both ρ and σ in terms of a generalized form of Ohm's law. To achieve this, two vector quantities must be introduced: the Electric Field (E [V/m]) and the Current Density (J $[A/m^2]$). These can be related to each other using ρ and σ. Furthermore, because this work deals with UD CFRP's, which are anisotropic materials, both ρ and σ take on the form of a second order tensor. This is to account for the fact that the conductivity in the fibre direction is significantly higher than in the directions transverse to the fibres. In this work, a tensor quantity is indicated by a bar added above the character. Considering $\bar{\rho}$ and $\bar{\sigma}$ in terms of the material coordinate system results in the tensorial form of Ohm's law:

$$\begin{Bmatrix} E_x \\ E_y \\ E_z \end{Bmatrix} = \begin{bmatrix} \rho_1 & 0 & 0 \\ 0 & \rho_2 & 0 \\ 0 & 0 & \rho_3 \end{bmatrix} \begin{Bmatrix} J_x \\ J_y \\ J_z \end{Bmatrix} \qquad (2.2)$$

$$\begin{Bmatrix} J_x \\ J_y \\ J_z \end{Bmatrix} = \begin{bmatrix} \sigma_1 & 0 & 0 \\ 0 & \sigma_2 & 0 \\ 0 & 0 & \sigma_3 \end{bmatrix} \begin{Bmatrix} E_x \\ E_y \\ E_z \end{Bmatrix} \qquad (2.3)$$

where the subscripts 1, 2, and 3 refer to the principal directions of the material coordinate system and the subscripts x, y, and z refer to the principal directions of the global coordinate system. Both of which are defined in Figure 2.2. One can tell from the units of E and J, that these expressions are closely related to the more well known form of Ohm's law: "$V = IR$". E represents a voltage over a certain distance (i.e. a potential difference). J, as can be inferred from its name, represents how much current is flowing through a plane; in the direction normal to said plane. In the case of $\bar{\rho}$, the diagonal terms give an indication of the magnitude of the electric field generated in a principal direction by a current density applied in the same direction. On the other hand, the off-diagonal terms indicate the magnitude of the electric field generated in a principal direction by a current density applied along another direction. Note that all off-diagonal terms are zero. This is the case when the material coordinate system and global coordinate system are fully parallel: $\theta = 0°$.

To define the tensors in terms of the global coordinate system, they must be generalized to account for the possibility of $\theta \neq 0°$. For this, a rotation matrix is used to perform tensor rotation about the z-axis. In this work the 3- and z-axes are always assumed parallel, and rotation is only possible about the z-axis. This means that the off-diagonal terms relating the 3-direction to any other direction are always zero. However, the off-diagonal terms relating the 1- and 2-direction to each other are not necessarily zero. Furthermore, the principal 3- and z-terms are not influenced by the rotation; they remain constant regardless of the θ. The

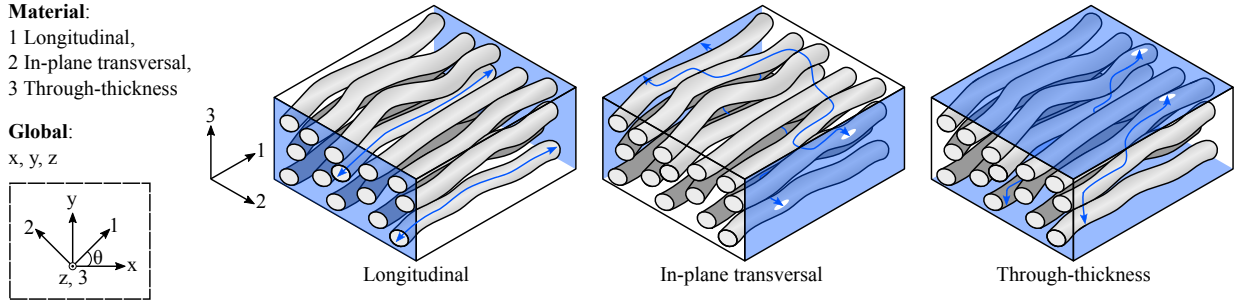

Figure 2.2: *Conductivity along the three principal directions inside a UD CFRP ply. Adapted from [2].*

general form of $\bar{\rho}$ then becomes:

$$\begin{aligned}\bar{\rho}_\theta &= \begin{bmatrix} c & -s & 0 \\ s & c & 0 \\ 0 & 0 & 1 \end{bmatrix} \begin{bmatrix} \rho_1 & 0 & 0 \\ 0 & \rho_2 & 0 \\ 0 & 0 & \rho_3 \end{bmatrix} \begin{bmatrix} c & s & 0 \\ -s & c & 0 \\ 0 & 0 & 1 \end{bmatrix} \\ &= \begin{bmatrix} c^2\rho_1 + s^2\rho_2 & cs(\rho_1 + \rho_2) & 0 \\ cs(\rho_1 + \rho_2) & s^2\rho_1 + c^2\rho_2 & 0 \\ 0 & 0 & \rho_3 \end{bmatrix} = \begin{bmatrix} \rho_{xx} & \rho_{xy} & 0 \\ \rho_{xy} & \rho_{yy} & 0 \\ 0 & 0 & \rho_{zz} \end{bmatrix}\end{aligned} \tag{2.4}$$

where c and s denote $\cos\theta$ and $\sin\theta$ respectively. The in-plane resistivity of a UD CFRP ply for any fibre orientation (θ) is thus defined. Note that when $\theta = 0°$, the tensor simplifies back to Equation 2.2. Also, when $\theta = 90°$, ρ_1 and ρ_2 switch position in Equation 2.2 because the 2-axis is now aligned with the x-axis. Note that $\bar{\sigma}_\theta$ will be structured similar to the generalised resistivity tensor, as a result of applying the same rotation matrix

To develop electrical models of CFRP materials, the electrical conductivity of the given material must be accurately measured. The electrical conductivity of a UD CFRP ply depends on the electrical conductivity of the carbon fibres and the fibre volume fraction of the composite. The latter is especially relevant for the in-plane transversal conductivity (σ_2), and the through-thickness conductivity (σ_3). Here, one could assume that the electrical conductivity is zero, because the plastic matrix insulates the conductive fibres. However, when tested experimentally, this is not the case. The slight electrical conductivity transverse to the fibres is caused by fibre-to-fiber contacts. The fibres inside the material are not perfectly straight and parallel to each other. In actuality, fibres can be wavy and come in contact with neighbouring fibres. Current is then able to flow from one fibre to the next, thereby resulting in an electrically conductive circuit. However, the electrical resistance encountered at fibre contacts is higher than the resistance inside the fibre.

The fibre network inside the composite can be thought of as an electrical circuit with many parallel paths of varying resistances. A current flowing through this parallel circuit would distribute itself over the circuit as a function of resistance encountered along the given path. Meaning that high resistance paths, where there are many fibre-to-fibre contacts for example, will have less current flowing through them. On the other hand, low resistance paths, which consist of mostly continuous fibres, will have more current flowing through them. This is analogous to the statement that "current always flows through the path of least resistance". Note that this statement is used throughout this work, and refers to this behaviour.

Essentially, Current flow through fibre contact is only favored when there is no direct path to a ground provided by continuous fibres. Increasing the fibre volume fraction can increase the number of contacts, thereby facilitating current flow in the 2- and 3-direction. The number of contacts largely depends on manufacturing process used and are distributed stochastically inside the material.[13–18]

Typically, the longitudinal electrical conductivity (σ_1) of CFRP's is determined through the Rule of Mixture (RoM):

$$\sigma_1 = \sigma_f v_f + \sigma_m v_m \approx \sigma_f v_f \tag{2.5}$$

where σ [S/m] represents an electrical conductivity, v [-] represents a volume fraction, and the subscripts f and m refer to the fibre and matrix respectively. The simplification is a result of the assumption that the polymer matrix is an electrical insulator (i.e. $\sigma_m = 0$). This provides a relatively fast and accurate manner to estimate σ_1. However, this is not enough to accurately determine the conductivities transverse to the fibres. These differ from the longitudinal conductivity because they depend highly on the underlying structure of the material as well as the material itself.

2.2 Measuring electrical conductivity

One way to determine the transverse conductivities, σ_2 and σ_3, is to directly measure them through experimental methods; or to measure the respective resistivity. Typically, this is done by attaching electrodes to a specimen and introducing a direct current (DC) to flow from one electrode to another. The voltage difference measured between two electrodes is then used to determine the electrical resistance (R) of the specimen in the tested direction through Ohm's law.

2.2.1 Experimental methods

In this work, a basic electrical contact is referred to as an electrode. A distinction is made between three types of electrical contacts: a terminal, a ground, and a probe. The terminal is the electrode from which the current is introduced into the material. The ground is the electrode through which the current exits the material. Probes come in pairs and are simply two electrodes used to measure a voltage difference between two points. Furthermore, because of the anisotropic electrical properties of the material, it is also crucial to clarify the idea of a 'test direction'. In this work, the x-axis of the global coordinate system coincides with the test direction. This is the general direction in which the current flows, and the direction in which the voltage differences are measured. An electrical property that is calculated directly from this data, is said to be directional and is denoted with a subscript x. This, for example, makes it possible to determine a unique ρ_x for any angle θ (see Figure 2.2).

There are many test methods used to measure voltage differences, among which: two-probe method, four-probe method, and six-probe method. The name 'six-probe' is somewhat deceiving when considering the manner in which probes are defined in this work. In actuality, a 'six-probe' method uses six electrodes, amounting to only two probes. Figure 2.3 visualizes a potential six-probe setup, where the two probes are shown as V_t and V_b. To reduce that setup to a four-probe one, the V_b probe can be removed. Alternatively, Figure 2.1 gives an example of a two-probe setup. The main drawback of the two-probe method, is that the terminal and ground also act as the probe. Essentially, they supply the voltage and measure the resulting current simultaneously. This can reduce the accuracy of the measurement. The largest issue lies in the fact that the resistance of the contacts is in series with the resistance of the material, and it can be difficult to separate the two contributions. The four-probe method gets rid of this issue by separating the voltage

probe from the terminal and ground, and placing it in parallel. Finally, the six-probe method goes one step further and adds another voltage probe; one on the top surface of the specimen and one on the bottom surface. This way, it can be checked whether there is a difference in the recorded voltage difference, and material inhomogeneities across the thickness of the specimen can be accounted for.

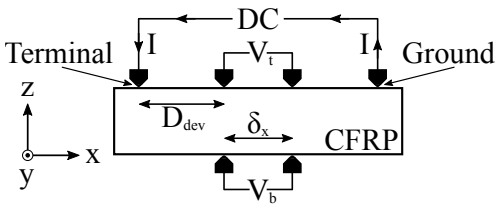

Figure 2.3: *Potential setup for six-probe method on a CFRP specimen using direct current (DC). A two-probe method would only include the terminal and ground. An example four-probe method could get rid of the V_b probe.*

In current literature, the four-probe method is most commonly used for CFRP materials. Athanasopoulous & Kostopoulos [13] measured the electrical resistivity of dry UD carbon fibre preforms with varying fibre orientations, aspect ratios (see Figure 2.5), and thicknesses. In all cases, two braided copper electrodes were attached at both ends of the specimen (top and bottom) and connected to a precision multimeter to measure the electrical resistance of the specimen. In subsequent work, Athanasopoulos et al. [19], measured the electrical resistance of dry UD carbon fibre preforms with varying number of layers and under several uniform pressure distribution. A similar method was used with two electrodes on both edges. Alternatively, different methods can be used to measure different directional conductivities. Park et al. [20] measured the electrical anisotropy of UD CFRP specimens by employing a six-probe method for the through-thickness conductivity, and a four-probe method for the transversal conductivity.

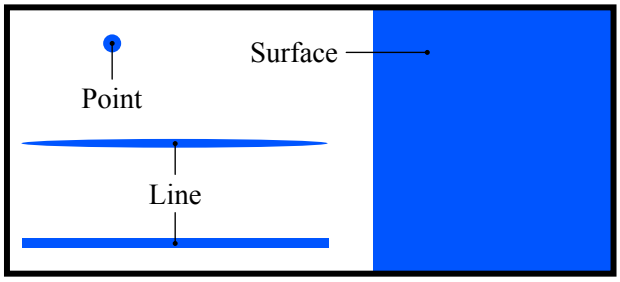

Figure 2.4: *Different types of electrode contacts used for electrical measurements.*

Independent from the number of electrodes used, is the type of contact the electrode has with the specimen: surface, point, or line. Firstly, a surface contact covers a face of the specimen, either partially or entirely. These are most commonly used for two-probe methods as shown in Figure 2.1 where both ends of the specimen are fully covered. In the case of UD CFRP specimens, placing a surface electrode on part of the top or bottom surface of the specimen could result in short circuits and unreliable data. Further causes and effects of short circuits are discussed in the following chapter. Secondly, a point contact is essentially a surface contact but much smaller. This gets rid of the issue of short circuits. However, when using point contacts the contacts must be precisely aligned on the specimen; all must have matching y-coordinates. For UD CFRP specimens this is even more crucial due to a phenomenon unique to anisotropic materials. This is discussed in Section 2.2.3. Lastly, a line contact covers a rectangular, or oval, area where length $\gg$ width. This can also avoid the issue of short circuits; however, special precautions must be taken as

outlined in Section 2.2.3. While not explicitly stated by the authors what type of contact is used for the electrodes, from the schematics provided in [13, 19, 20], it can be assumed that all electrodes form line contacts. Figure 2.4 summarises the different contact types found in literature.

2.2.2 Conductivity data found in literature

When it comes to principal conductivities or resistivities, longitudinal and in-plane transversal are by far the most reported on in literature. Through-thickness conductivity is often left out of the scope of the study.

Table 2.1: *Experimental results for directional electrical conductivity of UD CFRP materials and dry UD CF tows reported in literature. For exact values see reference.*

Material	Method	v_f [-]	σ_1 [S/m]	σ_2 [S/m]	σ_3 [S/m]	Reference
AS4/3501-6	16-probe	N/A	33,300	17	N/A	[21]
T700SC/2500epoxy	4/6-probe	0.59	N/A	5	4.5	[20]
T700SC,	4-probe	0.5	31,700	38	N/A	[13]
T700SC,	4-probe	0.5	31,600	42	N/A	[22]
C/E022epoxy	2/4-probe	0.6	44,300	50	N/A	[23]
AS4D/PEKK	2/4-probe	0.59	22,900	3	0.4	[24]
AS4/PEEK 16-ply	6-probe	0.59	38,300	11	1.3	[25]
AS4D/PEKK 16-ply	6-probe	0.59	36,900	4	0.7	[25]

Table 2.1 displays the electrical conductivity of UD CFRP laminates measured by several authors. Schueler et al. [21] are the only to have used more than six electrodes and also alternating current (AC) as opposed to DC. All reported values are averages of several specimens. In some cases, the value reported is converted from a resistivity to a conductivity for the sake of consistency. The exact material, layup, or dimensions are not always indicated by the authors. However, this is not required to see general trends. Similarly, the thickness of the specimens is only relevant for σ_2 and σ_3, and this has no influence on the measured σ_1. Some of the materials tested are dry carbon fibre tows, while others are consolidated laminates made of pre-impregnated carbon-polymer tapes. While it might not be possible to directly compare results from these specimens, they give a good indication of what amount of electrical conductivity can be expected. The measured conductivities of the same material are not necessarily reproducible; this is also expected. It has been shown throughout literature that the morphology of CFRP materials can vary drastically between manufacturers, or even batches of the same manufacturer. Because the electrical conductivity is highly dependant on the carbon fibre network inside the composite, it is logical that a different random arrangement can result in a different measured conductivity. What matters is the approximate magnitude of the directional conductivities themselves, as well as the magnitudes of the different principal directions relative to each other. For example, it is clear that σ_1 is always measured as being several magnitudes higher than σ_2 or σ_3. While σ_2 and σ_3 are within the same magnitude. This confirms that the fibre orientation is an important factor for the directional conductivity of the composite material.

2.2.3 Equipotentials

The current distribution inside the material is an important consideration when measuring electrical properties. In the case of UD CFRP materials, the extremely high conductivity of the carbon fibres can result in a non-uniform current distribution [20]. This is because the current favors flowing in the direction of the

fibres, where it faces considerably less electrical resistance. Therefore, the non-uniformity of the current distribution must be taken into account when using probes to measure voltage differences. It must be noted that this is only significant for $\theta \neq 0°$ and $\theta \neq 90°$. Another way to visualize this is by considering the equipotential lines, and their orientation within the material.

An equipotential is essentially a region in space in which the, in this case, electrical potential is constant. This can be in the form of a volume, surface, or line. For this work, the interest lies on equipotential lines. These are paths inside the material along which the voltage drop is relatively close to zero. This can be understood as a path where the electric current faces relatively little to no electrical resistance. Note that in practice, the resistance need not be zero, it simply needs to be low enough in comparison to other potential routes the current could take. As one can imagine, this phenomena is highly relevant when it comes to studying anisotropic composite materials.

No matter the physical circuit, the electric current will flow from the terminal where it is introduced, to the ground where it can be dissipated. The physical circuit of relevance in this work is the network of carbon fibres inside the composite material. The current has a multitude of potential paths which lead from the terminal to the ground. However, these paths are not equal in all aspects. The most important factor which dictates the preferred path is the extent of electrical resistance encountered along said path. As can be expected, lower resistance paths are preferred. Certain paths can have different sections with varying levels of electrical resistance. For example, in a network of carbon fibres, current can flow through a continuous fibre, but it can also flow between neighbouring fibres. The electrical resistance of the fibre is different from that of a fibre-to-fibre contact. While the continuous fibre path has lower resistance, if it does not directly run from terminal to ground, the current is forced to flow to other fibres to reach the ground. This occurs when $\theta > 0$ and is the reason that σ_2 and σ_3 are not equal to zero. Because the resistance encountered between fibres greatly exceeds that within the fibres, the formation of equipotentials inside composite materials is noticeably different when compared to isotropic materials. An example of current being forced to flow through fibre contacts is shown in Figure 2.2.

While measuring the electrical conductivity for several configuration types of CFRP materials, Athanasopoulous & Kostopoulos [22, 23] observed that for UD specimens "the equipotential lines tend to be directed along the fibres". Schueler et al. [26] also came to the conclusion that the fibre orientation inside UD CFRP materials determines the orientation of the equipotential lines. This claim is validated in COMSOL in the following chapter of this work. The implication of this is that probe placement can have a non-trivial effect on the measured electrical conductivity. However, all work reviewed did not explicitly take equipotentials into consideration during measurements, only as an observation after the fact. Furthermore, no other literature was found on the topic of probe placement, with respect to equipotentials, during electrical measurements for UD CFRP materials.

Another aspect of probe placement optimization found in current literature is regarding the zone in the specimen where the current flow is fully developed. To conduct reliable measurements, the voltage probes must be placed within this zone where the current is fully developed. The horizontal distance between the terminal and first electrode of either probe (D_{dev}), the through-thickness conductivity (σ_3), and the thickness of the specimen all affect this zone. One way to determine an appropriate D_{dev} for any given thickness and material, is to make use of the six-probe method as shown in Figure 2.3; increasing D_{dev} until $V_t = V_b$. Once this condition is met, it can be assumed that the current flow is fully developed. In the frame of this work, a fully developed current flow refers to a current distribution that is uniformly distributed over the cross-sectional area of the material. In their work, Park et al [20] considered the optimal distance

between the terminal and first electrode of the voltage probe to minimize measurement error. In this work, COMSOL is used for a similar purpose. This is also addressed in the following chapter.

2.2.4 Specimen geometry

Athanasopoulous & Kostopoulos [13], and Weber et al. [18] emphasize the importance of specimen dimensions and aspect ratio when measuring electrical conductivity of UD CFRP materials. Both claim that when measuring the conductivity of a specimen where $\theta > 0°$, it must be ensured that there is no direct path from the terminal to the ground. This is due to the carbon fibres acting as extremely low resistance pathways for the current. For example, if a specimen with fibres at $\theta = 45°$ has an aspect ratio such that some fibres run from terminal to ground, the results would resemble a specimen with fibres at $\theta = 0°$. The relevant aspect ratios are described in Figure 2.5. This means that electrode placement along the test direction (x-axis) can vary depending on the fibre orientation (θ). There exists a critical aspect ratio (λ_{cr}) for any given fibre orientation where fibres run from one corner of the specimen to the opposite corner, as in Figure 2.5 (a). This results in a small subset of paths being preferred. For an aspect ratio which it too small, as in Figure2.5 (c), fibres can run directly from terminal to ground which will also influence the conductivity measurement. On the other hand, for an aspect ratio which is too large, there might not be enough random fibre contacts for proper electrical conductivity. The ideal specimen would thus have an aspect ratio as in Figure 2.5 (b), where there is no direct path from terminal to ground. Theoretically, aligning the electrodes with the fibre direction could prove helpful here. Essentially, this makes it impossible for fibres to run directly from the terminal to the ground. Further implications of this are discussed in the folowing chapter.

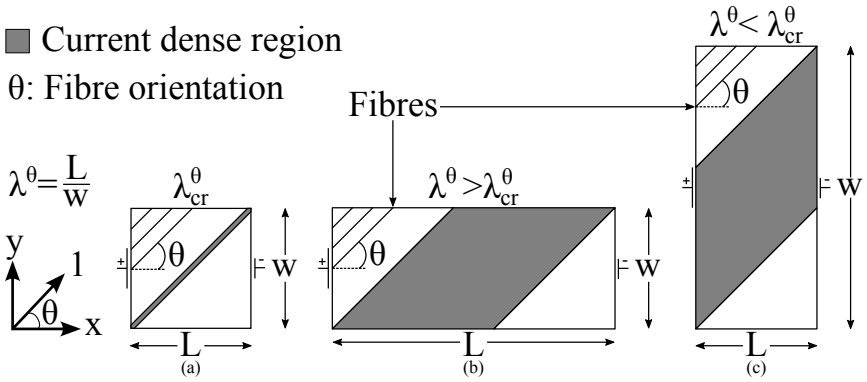

Figure 2.5: *Specimen geometry and relevant aspect ratios: (a) critical aspect ratio, (b) desired aspect ratio, (c) too small aspect ratio. In all cases the terminal is on the left and the ground on the right. Adapted from [13].*

2.3 Analytical expressions

Before Equations 2.2 and 2.3 can be used, the individual terms of E and J must be defined. Because of the way the test direction is defined with respect to the global coordinate system in this work, J_y can be taken as zero. The current is always set to flow in the direction of the x-axis, meaning that the current density only consists of an x-component. Figure 2.6 (a) displays how the current density and its relevant components stay consistent regardless of fibre orientation. Furthermore, this work considers how the fibre orientation influences the conductivity along the test direction. Out-of-plane contributions thus have no influence on this.

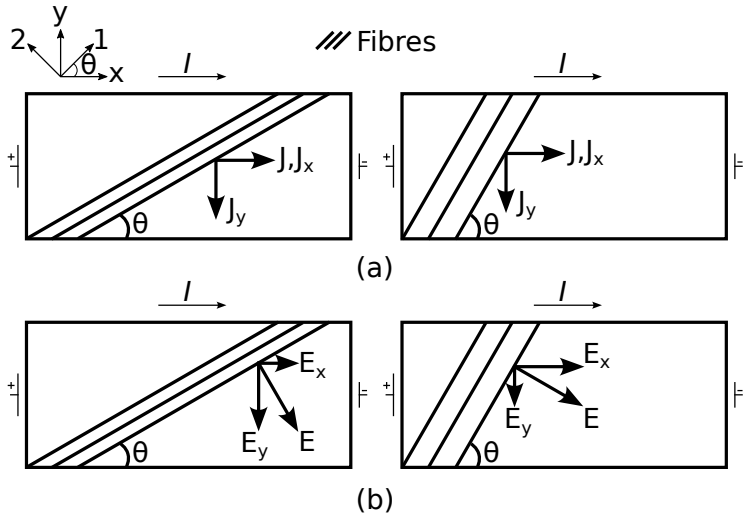

Figure 2.6: *Sketch of the (a) current density components and (b) electric field components during off-axis measurement. The current density runs parallel to the test direction. The chosen test direction in this work is the x-direction. Therefore, J only consists of J_x, while $J_y = 0$. The electric field lies perpendicular to the fibres. Therefore, E consists of E_x and E_y.*

Equation 2.2 then simplifies to:

$$\begin{Bmatrix} E_x \\ E_y \end{Bmatrix} = \begin{bmatrix} \rho_{xx} & \rho_{xy} \\ \rho_{xy} & \rho_{yy} \end{bmatrix} \begin{Bmatrix} J_x \\ J_y \end{Bmatrix} \tag{2.6}$$

where $J_y = 0$. This leaves the following components to be defined:

$$E_x = \frac{\Delta V}{\delta_x} \qquad (2.7) \qquad J_x = \frac{I}{A} \qquad (2.8) \qquad E_y = \frac{E_x}{-t} \qquad (2.9)$$

where I [A] is the current applied, and t denotes $\tan\theta$. Note that E_y follows from the Pythagorean theorem. This is clarified in Figure 2.6 (b). Substituting Equations 2.4, 2.7, 2.8, and 2.9 into Equation 2.6 results in the following two expressions:

$$\rho_{xx} = c^2\rho_1 + s^2\rho_2 = \frac{E_x}{J_x} = \frac{RA}{\delta_x} \qquad (2.10) \qquad \rho_{xy} = cs(\rho_1 + \rho_2) = \frac{\rho_{xx}}{-t} \qquad (2.11)$$

where R [Ω] follows from Ohm's law. Essentially, a current is applied to the material, and the resulting voltage difference over the material is measured. This allows one to determine the electrical resistance of a material with $V = IR$. Equations 2.10 and 2.11 make it possible to compare an expected resistivity to a measured resistivity. Furthermore, because $\rho_1 \ll \rho_2$, the ρ_1 term can be neglected in both expressions. This makes it possible to determine ρ_2 and σ_2 from experimental data:

$$\rho_2 = \frac{1}{\sigma_2} = \frac{RA}{s^2\delta_x} \tag{2.12}$$

2.3.1 Measuring considerations

In this Chapter, a multitude of relevant aspects that can influence electrical resistivity measurements have been considered. Since such measurements are also carried out in this work, there is value to summarising the most important points. The following is a list of guidelines which must be taken into account when conducting electrical measurements on UD CFRP materials:

1. Use a minimum of four electrodes (terminal, ground, and one probe 'set').
2. Use an electrode contact type that suits the specimen dimensions, and allows the intended conductivity to be measured. Alignment between electrodes, or with respect to the fibre orientation, must be considered when using point- or line-contact electrodes.
3. Use a specimen aspect ratio based on the purpose of the measurement. This will dictate which principal, in-plane, conductivity dominates.
4. Prepare specimens such that there is sufficient horizontal distance for the current flow to fully develop between the terminal and first electrode of either probe. This ensure the measurement is done within a zone of uniform current distribution.

Decisions made for the models and experimental setup used in this work are based on these guidelines. Note that these are specifically intended for UD laminate composites. Chapter 4 outlines all details relating to the experimental methods employed in this work. However, before reliable measurements can be done, a number of claims made in this chapter must first be tested, explained, and validated.

Chapter 3

Modelling

To develop a reliable test method, the measuring considerations discussed in the previous chapter must be fully explored. To this end, this chapter utilizes numerical modeling to visualize relevant phenomena and validate assumptions. The advantage of using a model lies in the fact that this is an iterative process, where adaptations can be made to the model and the resulting changes can be measured and compared. The model essentially has a tighter feedback loop than a physical experimental setup; making the time between attempts shorter. A 2D model is built in COMSOL to investigate the stated measuring conditions. A 3D model is then used to validate the assumption that a 2D model is sufficient to describe the electrical behaviour of a UD laminate.

3.1 Model design

The aim of the model is to simulate how current flows through a given material. For said model to be functional, a number of inputs are necessary. These inputs have been arranged in the following three categories:

- Geometry:
  - Specimen length (L) [mm]
  - Specimen width (w) [mm]
  - Specimen thickness (h) [mm]
  - Fibre orientation (θ) [°]
  - Distance between terminal and first electrode of voltage probe (D_{dev}) [mm]
  - Distance between electrodes of voltage probe (δ_x) [mm]
- Material properties:
  - Electrical conductivity tensor ($\bar{\sigma}$) [S/m]
  - Relative permittivity (ϵ) [-]
- Model inputs:
  - Applied voltage (V_{in}) [V]

Once these inputs have been defined, a voltage difference is applied across the material so that the resulting behavior can be analyzed. The model can then be used to investigate several material configurations and relationships between parameters. Parametric sweeps are the ideal tool for this. For a basic parametric sweep, the model is run multiple times where on each iteration, a pre-determined variable is changed while all others are kept constant.

No rigorous validation has been performed on COMSOL. A simple comparison between results from analytical expressions and simulated results was done. For example, it is expected that COMSOL performs tensor rotations on the conductivity tensor to convert the input conductivity to an apparent conductivity which depends on θ. For the model to be valid, the conductivity of the model must match the conductivity predicted by the analytical equations. The apparent conductivity tensor was calculated in MATLAB for varying fibre orientations according to Equation 2.2. Next, a model of a material with a the same base conductivity tensor was built in COMSOL; and a parametric sweep was carried out over the same range of fibre orientations. COMSOL allows the user to query the individual components of the conductivity tensor for each iteration. These values were identical to the values calculated in MATLAB. Furthermore, E_x and J_x can also be queried within COMSOL. For example, in Figure 3.1, one can determine the E_x at any point on the surface of the specimen. Alternatively, E_x and J_x can be calculated using Equations 2.7 and 2.8 respectively. Comparing these two methods results in very similar values for E_x and J_x. It is thus assumed that the model is valid.

Before the first model can be built, decisions must be made regarding guidelines 1 and 2 from the measuring considerations. First, it is recommended to use a minimum of four electrodes, including one probe set. To account for material inhomgeneities during physical testing, the choice is made to use an extra probe set at the bottom of the specimen. This results in six electrodes, also referred to as a six-probe method. Secondly, the electrode contact type must be chosen. The surface contact electrode is not suitable for the probe electrodes. The point contact, while suitable, is not commonly used. The line contact is the most common, and also allows one to investigate the effects of electrode and fibre (mis)alignment. Therefore, the line contact electrodes are used.

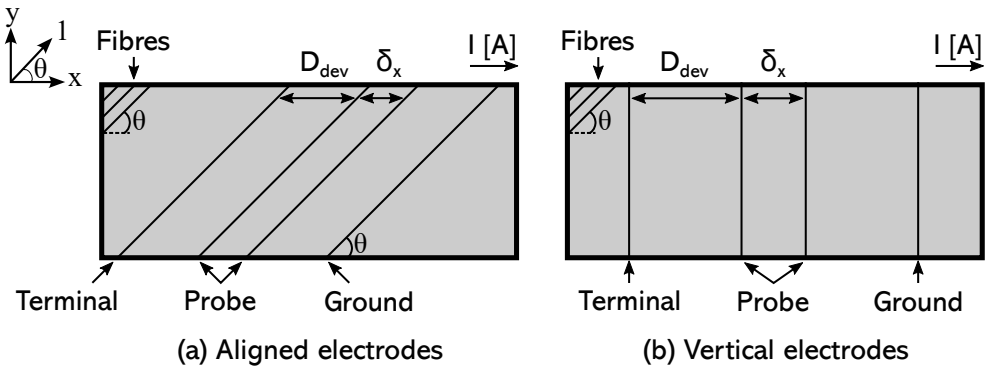

Figure 3.1: *The two types of electrode configurations used in this work.*

In a 2D model, the top and bottom probes are the same, meaning that only four electrodes are modeled. Figure 3.1 gives an example of the potential layouts of a 2D model. The implications of using (a) aligned electrodes or (b) vertical electrodes is discussed in Section 3.3. The model is built in such a way that changing the input θ applies a tensor rotation to adjusts the input $\bar{\sigma}$. For the model with aligned electrodes, θ also defines the electrode orientation. Note that D_{dev} and δ_x are always measured in the test direction. Furthermore, it must be noted that the specimen is modelled as a homogeneous piece of material. This means that

the fibres and matrix material are not modeled separately. For example, when it is stated that current flows along the fibres, what is meant is that the current flows in the 1-direction. This direction is defined by the input θ.

3.2 Specimen in-plane dimensions

Guideline 3 of the measuring considerations requires the aspect ratio (λ^{θ}) of the specimen to be further investigated. This ratio is defined as the length of the specimen divided over the width of the specimen. This was also shown in Figure 2.5. For the sake of clarity, the edges of the specimens are labeled with respect to the view. The relevant edges are indicated in Figures 3.2-3.4.

3.2.1 Relevant aspect ratios

As was described in Section 2.2.4, there exists a critical aspect ratio (λ^{θ}_{cr}), for every fibre orientation angle (θ), where continuous fibres run from one corner of the specimen to the opposite corner. As θ increases, the value of this ratio decreases. Three examples of specimens with a critical aspect ratio are shown in Figure 3.2. λ^{θ}_{cr} is used to split the possible aspect ratio of the specimen into three categories. The first of which is simply $\lambda^{\theta} = \lambda^{\theta}_{cr}$.

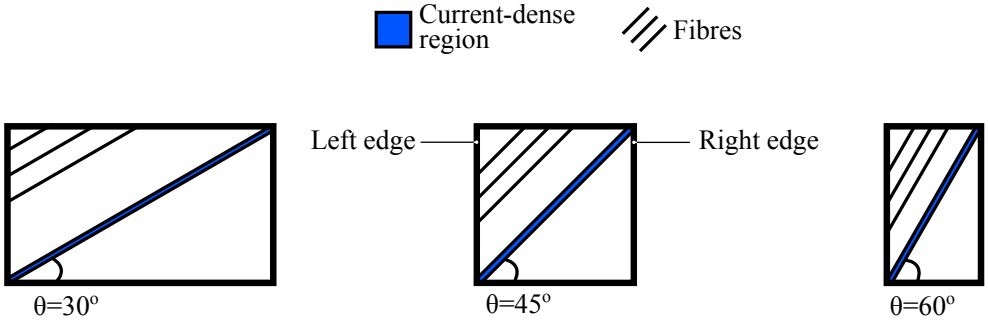

Figure 3.2: *Example specimens for which* $\lambda^{\theta} = \lambda^{\theta}_{cr}$.

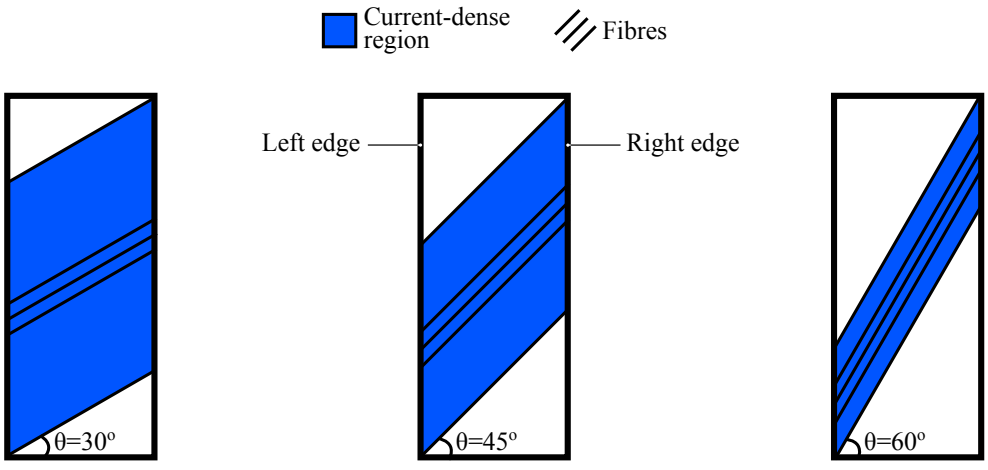

Figure 3.3: *Example specimens for which* $\lambda^{\theta} < \lambda^{\theta}_{cr}$.

The second category consists of specimens with an aspect ratio which is smaller than the critical aspect

ratio. Note that λ_{cr}^{θ} always depends on the fibre orientation. For these specimens, a large number of continuous fibres run from the left edge of the specimen to the right edge. Specimens shown in Figure 3.2 only have fibres running along the diagonal. When $\lambda^{\theta} < \lambda_{cr}^{\theta}$, the number of fibres that provide a direct path from the left edge to the right edge increases. Examples of specimens with this aspect ratio are include in Figure 3.3. The same three fibre orientations as in Figure 3.2 are used.

The final category consists of specimens with an aspect ratio which is larger than the critical aspect ratio. What sets these specimens apart from the other two is that there are no fibres which directly run from the left edge to the right edge. Current which is introduced on the left edge must therefore flow through fibre contacts to reach the right edge. Once again, an example is given for the same three fibre orientations. This can be seen in Figure 3.4.

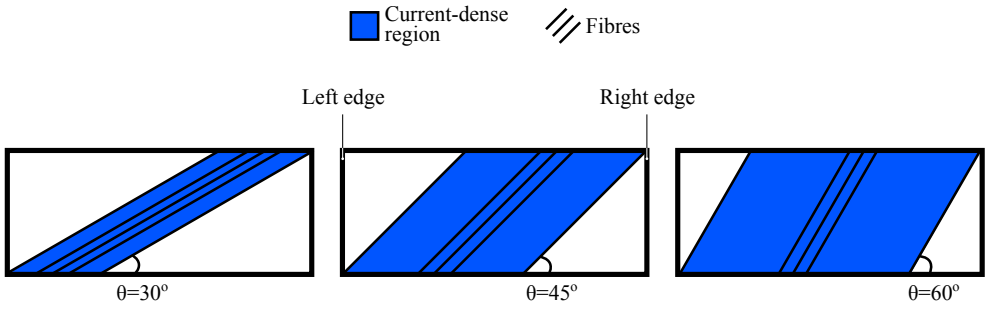

Figure 3.4: *Example specimens for which* $\lambda^{\theta} > \lambda_{cr}^{\theta}$.

Specimens where $\lambda^{\theta} \leq \lambda_{cr}^{\theta}$ contain fibres that provide a direct path between terminal and ground. This is essentially a short circuit. Because the conductivity along the fibres is several magnitudes higher than through fibre contacts. It is thus expected that these aspect ratios behave similarly because σ_1 is dominant in these scenarios. On the other hand, it is expected that specimens with an aspect ratio larger than the critical aspect ratio display drastically different electrical behaviour. Since the short circuit has been removed, σ_2 now becomes dominant. These three aspect ratios have been recreated in COMSOL to determine how the current density and equipotentials are affected.

In all three cases, a fibre orientation of 45° is used. Once again, note that the material is modelled as homogeneous, and there are thus no actual fibres. The simulated current density, and equipotential orientations, follow from the input $\bar{\sigma}$ which has been rotated according to θ. The latter always runs parallel to the fibre orientation (θ). The specimen is given a conductivity of $\sigma_1 = 40000$ [S/m] and $\sigma_2 = 10$ [S/m]. The vertical electrodes configuration shown in Figure 3.1 (b) is used. The electrodes make contact with the specimen along its entire width. The left edge is the terminal and the right edge is the ground. A potential difference of 60 [V] is applied across each specimen. The resulting current density has been plotted as streamlines over the surface of the specimen. Additionally, the resulting voltage distribution is plotted as a filled contour plot over the surface of each specimen. The equipotential zones are visualized by the color map in each plot. Only ten distinct voltage steps are used in order to keep the orientation of these zones clear. As the number of steps increases, the zones would approach lines, but would keep their orientation. Therefore, ten steps is enough to visualize the orientation of the equipotential lines. All this can be seen in Figures 3.5-3.7.

3.2.2 Specimen category 1: $\lambda^{\theta} = \lambda^{\theta}_{cr}$

In the case of a fibre angle of 45°, the critical aspect ratio is achieved by having a square specimen. The chosen dimensions are 40 [mm] by 40 [mm]. The resulting current distribution can be seen in Figure 3.5 (a), and the voltage distribution is shown in Figure 3.5 (b).

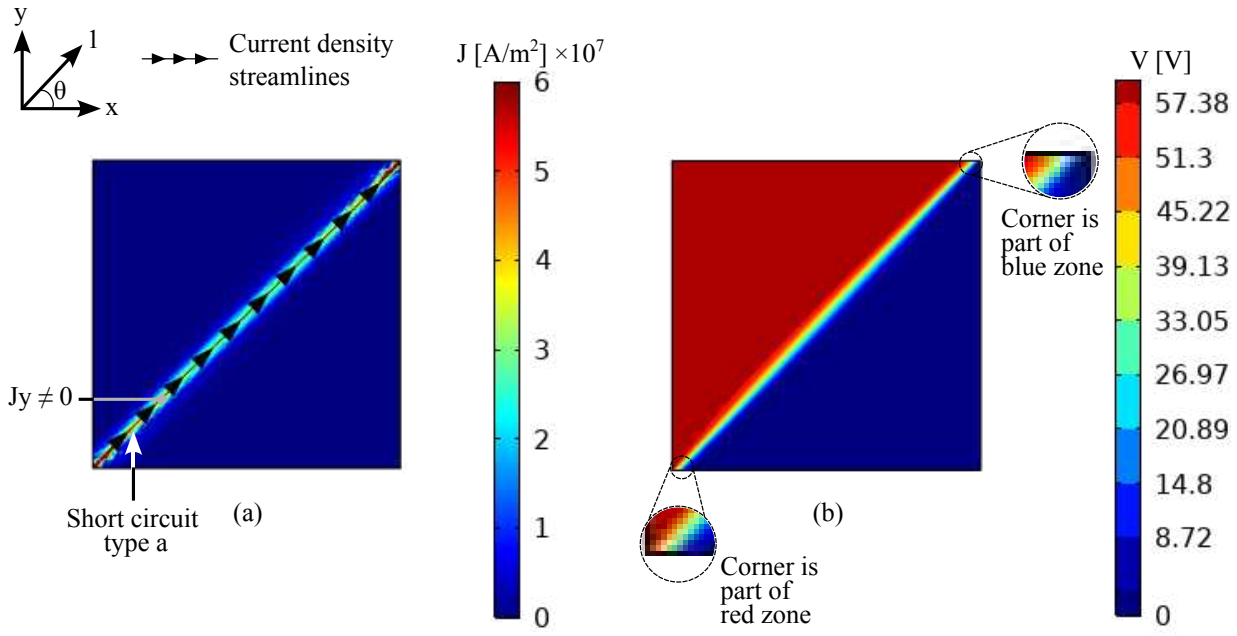

Figure 3.5: *Simulated (a) current distribution and (b) voltage distribution for specimen with the critical aspect ratio (λ^{θ}_{cr}).*

From the current distribution, one can tell that the majority of the specimen does not have any current running through it. Even though the entire left and right edge are electrical contacts, all current flows along the diagonal. This is because the current flows along the path where it encounters the least electrical resistance. Because of the prescribed fibre orientation (θ), the orientation of the diagonal coincides with the 1-direction. Along this diagonal, σ_1 dominates, and there is no need for the current to flow in the 2-direction at all. Thus, a highly preferred path is created. This path is essentially a short circuit, and is referred to as a 'type a' short circuit in this work. This type of short circuit occurs when one can draw a straight line, that runs parallel to the fibre orientation (θ), from the terminal (left edge) to the ground (right edge).

When looking at the voltage distribution, the diagonal once again stands out from the rest of the specimen. Since there is no flow of current in the top left or bottom right corners, the potential remains constant there. Along the diagonal, thin equipotential zones can be seen. These zones, where the simulated potential is constant, are oriented in the same general direction as θ, but are not exactly parallel to the 1-direction. Additionally, the equipotential zones are slightly curved. This is crucial, and it has been highlighted in Figure 3.5 (b). The bottom left corner is part of the high potential (red) zone, while the top right corner is part of the low potential (blue) zone. This means the the equipotentials are not oriented at 45°. They actually form a slightly larger angle with the x-axis.

Because the specimen has a critical aspect ratio, a straight line, that runs parallel to the fibre orientation (θ), can be drawn from the bottom left corner to the top right corner. One could assume that all current

should flow along the 1-direction from the bottom left corner to the top right corner. However, this line is one-dimensional, meaning it has no thickness. Simulating this flow of current is not possible in such a 2D model. Therefore, the current is actually forced to flow slightly in the 2-direction. This results in these equipotential zones which are seemingly parallel to the 1-direction.

In practice, this aspect ratio assumes a single fibre to run from the bottom left corner to the top right corner. This is not a realistic specimen. It is therefore only useful for modeling purposes. If it were to be used for resistivity measurements, the measured value would not provide much insight. This aspect ratio should thus not be used, regardless of which resistivity is being tested for: ρ_1, ρ_2, or ρ_{xx}.

3.2.3 Specimen category 2: $\lambda^\theta < \lambda^\theta_{cr}$

For the specimen with aspect ratio smaller than the critical aspect ratio, the width is kept at 40 [mm] while the length is decreased to 20 [mm]. The resulting current distribution can be seen in Figure 3.6 (a), and the voltage distribution is shown in Figure 3.6 (b).

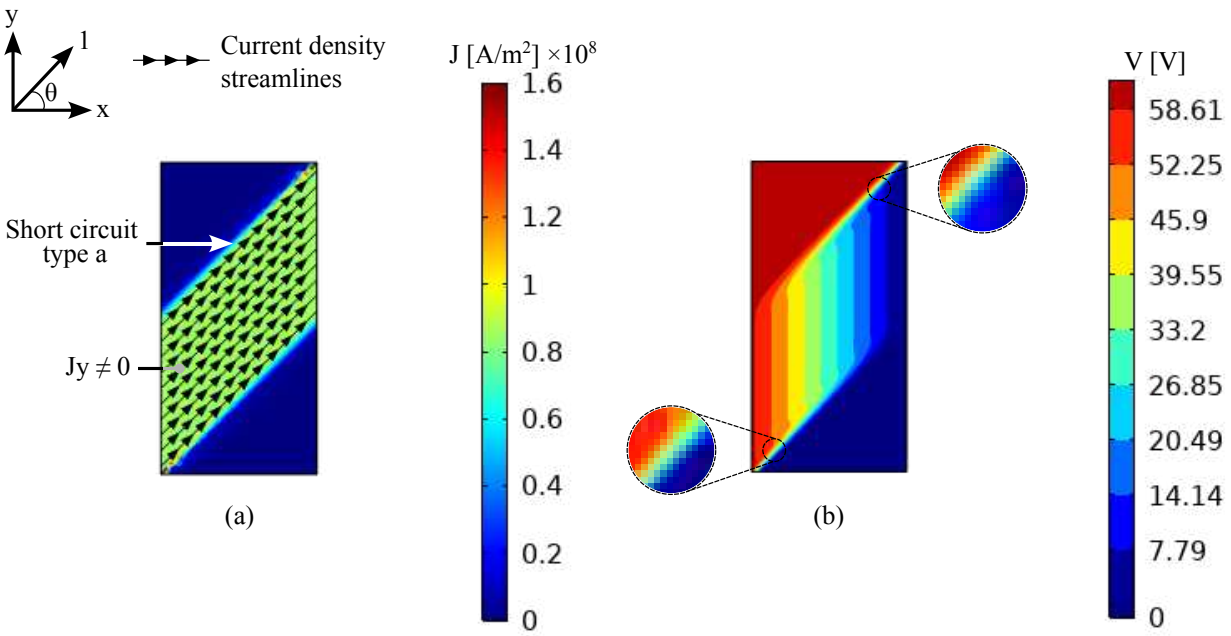

Figure 3.6: *Simulated (a) current distribution and (b) voltage distribution for specimen with an aspect ratio smaller than the critical aspect ratio ($\lambda^\theta < \lambda^\theta_{cr}$).*

This aspect ratio also results in a 'type a' short circuit. However, a much larger length of the left and right edge have current flowing between them. The concept is the same, the current flows there because it can take advantage of the low resistance encountered when flowing in the 1-direction. There is no need to flow in the 2-direction at all in this case. The small amount of flow in the 2-direction caused by the zero-thickness issue in the previous case is no longer present here. Note that the color map in Figure 3.6 (a) has a different range than the one shown in Figure 3.5 (a). This is done intentionally to keep the center, current dense region, at around the mid-point of the color map range.

Once again, the current dense zone is also highlighted in the voltage distribution plot. The equipotential zones are now mostly vertical (aligned with the y-direction). However, as is shown in Figure 3.6 (b), the top and bottom edges of the equipotential zones seem to run in the direction of θ. Essentially, if the region with vertical equipotensials were to be removed from Figure 3.6 (b), one would be left with Figure 3.5 (b). It thus seems that at the top and bottom edge of Figure 3.6 (b), the same 'zero-thickness' phenomenon is simulated. In the region with vertical equipotentials, ρ_1 fully dominates and there is absolutely no current flow in the 2-direction. Therefore, as the current flows in the 1-direction the voltage drops only depend on the distance traveled along this direction. Note that this is a direct result of Equation 2.1, which states that the experienced resistance increases proportionally with the length of the material. In this case, the length of the material is the distance traveled in the 1-direction.

Because the current is essentially flowing in the 1-direction from terminal to ground, it is expected that the measured ρ_{xx} is close to ρ_1. Essentially, ρ_2 does not contribute in this case. Therefore, such an aspect ratio could be useful for measuring the longitudinal resistivity of a material. To use this aspect ratio for measuring the in-plane transversal resistivity, one would have to re-define the test-direction, or make use of electrodes with point contacts. Both would prevent continuous fibres to run directly from terminal to ground. The same can be said for off-axis measurements: this aspect ratio is not suitable with the currently defined test-direction and electrode contact type.

3.2.4 Specimen category 3: $\lambda^\theta > \lambda^\theta_{cr}$

For the specimen with aspect ratio larger than the critical aspect ratio, the width is also kept at 40 [mm] while the length is now increased to 80 [mm]. The resulting current distribution can be seen in Figure 3.7 (a), and the voltage distribution is shown in Figure 3.7 (b).

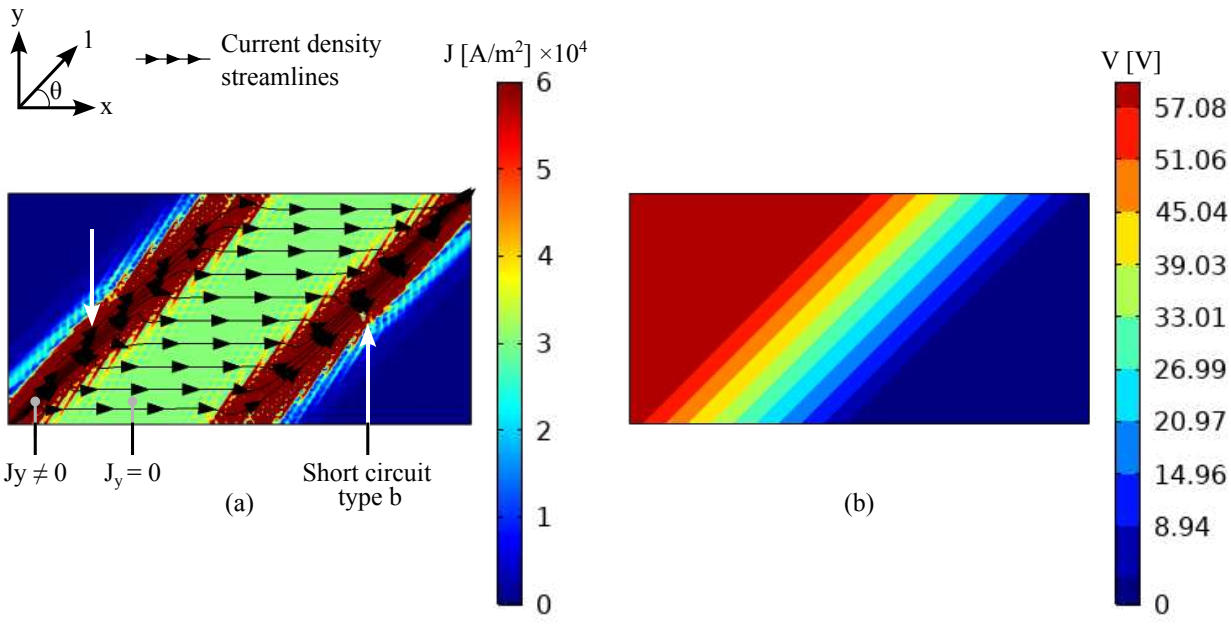

Figure 3.7: *Simulated (a) current distribution and (b) voltage distribution for specimen with an aspect ratio larger than the critical aspect ratio ($\lambda^\theta > \lambda^\theta_{cr}$).*

Specimens with this aspect ratio are no longer subject to 'type a' short circuits. This is because no straight line, that runs parallel to the fibre orientation, can be drawn between the left and right edge of the speci-

men. This means that current is forced to flow in the 2-direction to reach the ground. This can also be seen in Figure 3.7 (a), where the current density lines in the center no longer run along the 1-direction.

This does raise the issue of the red regions in Figure 3.7 (a). The current density there is twice as high as at the center of the specimen. This is because all the current flows through a small area. The current density streamlines clearly show this behaviour. In the center zone ($\approx 3 \times 10^4\ [A/m^2]$), the streamlines are well distributed. However, on the edges ($\approx 6 \times 10^4\ [A/m^2]$), there are many overlapping streamlines. It must be noted that the arrowheads have been normalized for this plot, because the difference in magnitude between the arrows in the red and green regions was too large. These overlapping streamlines indicate another type of short circuit. This is referred to as a 'type b' short circuit in this work. Here, the vertical electrodes are the cause of the short circuit. These short circuits flow in the direction of the fibre orientation. This occurs due to the same reason it occurs in the other specimen categories. The only difference being that in this specific case, the short circuit ends before it reaches the ground. The current is thus forced to flow along the 2-direction once it can no longer take advantage of the high conductivity along the 1-direction.

Figure 3.7 (b) clearly shows equipotential zones which are oriented parallel to the fibre direction. Furthermore, because current is forced to flow along the 2-direction, the simulated ρ_{xx} is expected to give a much better indication of the actual resistivity than the other two specimen categories.

3.2.5 Chosen aspect ratio

In all three cases, the simulated current dense regions match the expected current dense regions. This again indicates that the COMSOL model is functioning properly. The simulation results clearly indicate the presence of short circuits. Some of these are likely to influence conductivity/resistivity measurements on UD laminates with off-axis fibre orientations. Firstly, the critical aspect ratio is close to unattainable in practice. This aspect ratio is likely to result in a specimen that behaves similar to having an aspect ratio slightly larger or smaller than the critical aspect ratio. Secondly, specimens where $\lambda^\theta < \lambda^\theta_{cr}$ will find most of their value in measurements that test the longitudinal resistivity. This is due to the 'type a' short circuit. Lastly, specimens where $\lambda^\theta > \lambda^\theta_{cr}$ are the most suited for off-axis measurements. This is because there are no short circuits between the terminal and the ground, and ρ_{xx} is affected by ρ_2. For the other two aspect ratios, the ρ_2 term in Equation 2.10 has little to no contribution.

Furthermore, it is clear from the streamlines that there are regions where J only consists of a x-component, unlike with the two other aspect ratios. This is also a requirement when considering physical measurements, as Equations 2.10, 2.11, and 2.12 are based on the assumption that $J_y = 0$. In the following sections, the issue of $J_y \neq 0$ is addressed.

The final point considers the short circuit present in Figure 3.7. This short circuit is caused by how the terminal and ground electrode make contact with the specimen, with respect to the fibre orientation. To better understand why this happens, and the implications of this, the measuring consideration regarding electrode alignment for line contact electrodes is discussed next.

3.3 Electrode alignment

Now that it has been demonstrated what type of aspect ratio is favored, the following measuring consideration concerns the alignment of the line-contact electrodes with the fibre orientation. To investigate this, both the aligned and vertical electrodes configuration, shown in Figure 3.1, are used. A specimen with an

aspect ratio larger than the critical aspect ratio is modelled. The width is kept at 40 [mm]; however, the length is increased to 150 [mm]. Increasing the length of the specimen makes certain phenomenon appear more clearly in the results. At this stage the exact dimensions of the specimen do not matter yet, only that $\lambda^{\theta} > \lambda^{\theta}_{cr}$. Apart from this, the electrical properties, fibre orientation, and applied voltage are all kept constant with respect to the simulations done in the previous section.

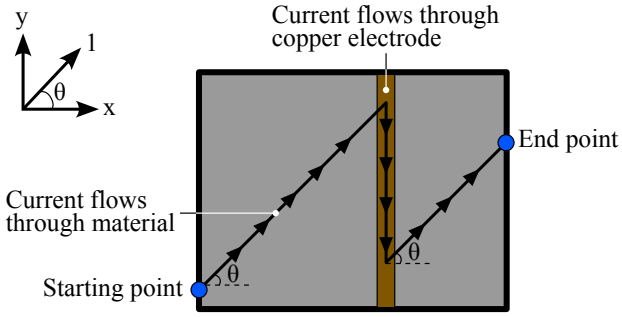

Figure 3.8: *Example of a 'type c' short circuit. The current flows through the hihgly conductive electrode to reach the end point without needing to flow in the 2-direction in the material itself.*

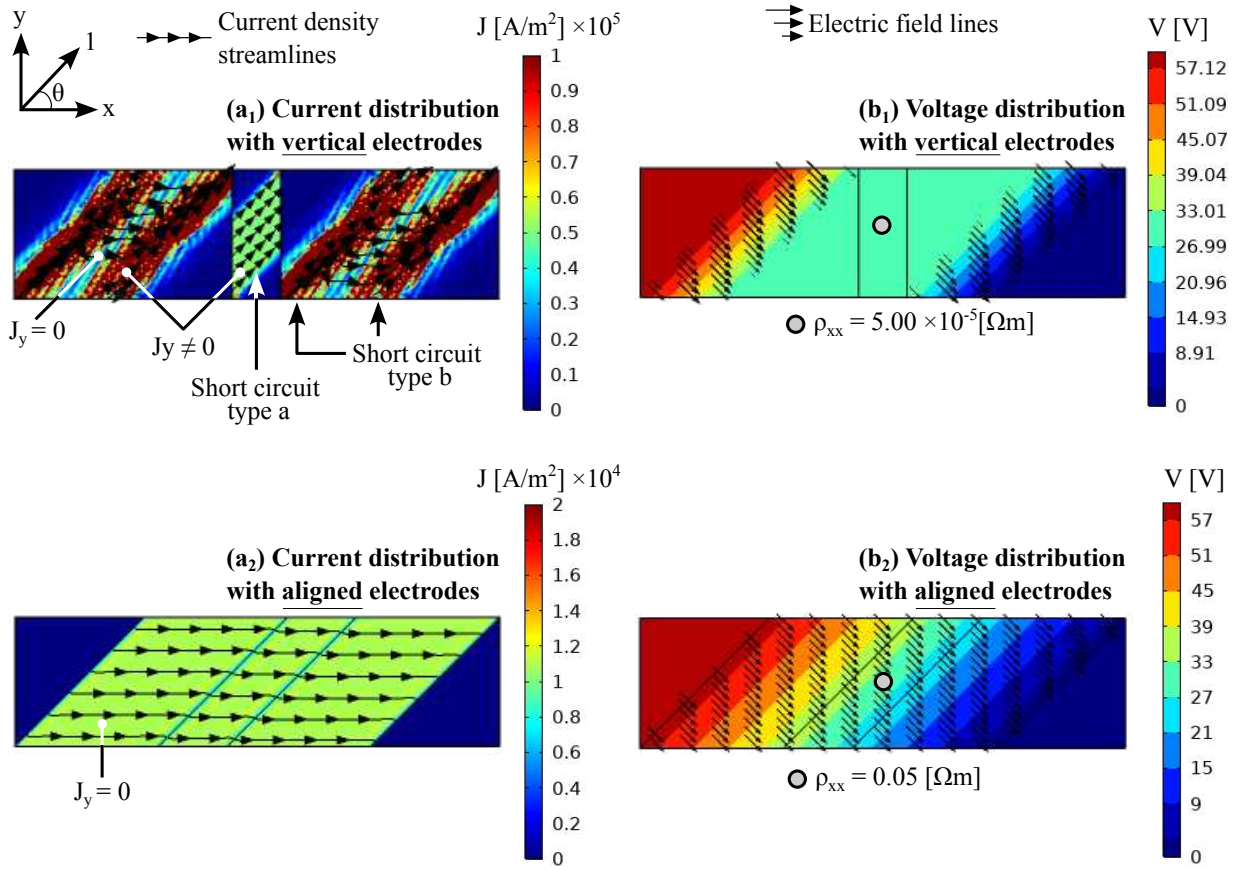

Figure 3.9: *Simulated (a) current distribution and (b) voltage distribution for measurement setup with (1) vertical electrodes and (2) aligned electrodes.*

In a 2D model, with a top down view, the electrodes are modeled as lines. These boundaries have no phys-

ical dimensions apart from a length. While these can be assigned certain material properties, these do no influence the simulation results without the use of an additional boundary condition. In this case, the 'Floating Potential group' boundary condition was used for the probe electrodes. Essentially, this makes the selected line segment into an isopotential/equipotential. This is also what would happen in physical experiments. The extremely high electrical conductivity of the copper electrodes ensure that the entire contact area between specimen and electrode becomes an equipotential zone. This is simply because the current can flow to any spot in the contact area by flowing from the specimen, into the electrode, and then back into the specimen. This creates a new type of short circuit, referred to as a 'type c' short circuit in this work. This has been visualized in Figure 3.8. This was not an issue in the previous simulations because the electrodes were not added to the model. However, these are now included to truly assess how electrode alignment can influence resistivity measurements of UD laminates. The simulated current distribution is shown in Figure 3.9 (a_1) for the vertical electrode configuration, and (a_2) for the aligned electrode configuration.

Here, a significant difference can be seen between the two electrode configurations. First of all, the vertical electrodes cause a multitude of short circuits. All three short circuit types are present; however, 'type c' cannot be visualized properly here. Furthermore, the 'type b' short circuits have doubled from Figure 3.7 (a). This is because the probe electrodes now also cause the same short circuit as the terminal and ground. Inside these red regions, the current density is extremely high, and the streamlines show a lot of overlap. As was explained before, this is because the current can flow in the 1-direction with no need to flow in the 2-direction. The highly preferred path ends when the current can no longer avoid flowing in the 2-direction. This is analogous to current flowing along fibres (1-direction) where electrical conductivity is significantly higher, instead of flowing transverse to the fibres (2-direction) where electrical conductivity is relatively low. When looking at the left or right side of the specimen, there is also a region between the two short circuit regions. This region with lower current density is a region where the current is forced to flow in the 2-direction. This is the reason a longer specimen was modeled. If the specimen is too short, the short circuit regions could overlap and the low current density region would disappear. If the length between the terminal and first electrode of the probe, or ground and second electrode of the probe, is short enough, one would end up with a 'type a' short circuit. Where there is a straight line path, oriented at θ, from terminal to electrode, and from electrode to ground. A similar 'type a' short circuit can already be seen in Figure 3.9 (a_1). This one is between the electrodes of the probe. If one only looks at this region between the electrodes of the probe, it looks very similar to Figure 3.6 (a). Both show the same electrical behaviour. A measurement done on this setup takes into account the conductivity of the electrodes, as opposed to the in-plane transversal conductivity of the specimen.

When looking at the aligned electrode configuration in Figure 3.9 (a_2), it is clear that all short circuits have disappeared. Here, the range of the color map is once again adjusted. Note that the type c short circuit is actually still present. However, the equipotential created by the copper electrode contact is now aligned with the fibre orientation. This can be seen in Figure 3.9 (b_2). In Figure 3.9 (b_1), the vertical electrodes completely alter the voltage distribution. The entire middle region has become an equipotential zone. This is because of the short circuits provided by the copper electrodes. Note that the edges of the zone still follow the fibre orientation. A way to interpret this is that once the current is within this large center region, it can flow to anywhere in this region with relative ease. The manner in which it does this explained by the 'type c' short circuit shown in figure 3.8.

Having discussed the current density, it is also valuable to understand how the electric field behaves inside UD laminates with off-axis fibre orientations. From Figure 3.9, it can be seen that the electrode alignment

has no impact on the orientation of the equipotential zones. These remain parallel to the fibre orientation. By definition, the electric field always points normal to the equipotential lines, even in anisotropic materials. To visualize this, two more fibre orientations were simulated. All other parameters are kept constant. The model was run with aligned electrodes, and the resulting voltage distribution is shown in Figure 3.10.

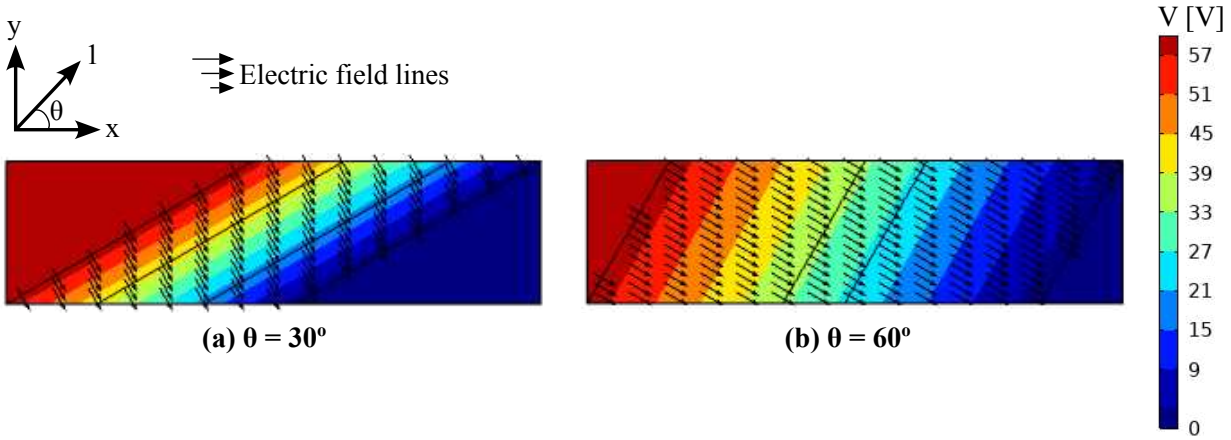

Figure 3.10: *Simulated voltage distribution for (a) fibre orientation of 30°, and (b) fibre orientation of 60°.*

As can be seen, the fibre orientation determines the equipotential orientation. This observation is in line with what was found in [22, 23, 26]. In all cases, the electric field is perpendicular to the equipotentials. This also means that *E* always has a contribution from both E_x and E_y when $0° < \theta < 90°$. These can be related to each other through the Pythagorean theorem using the fibre orientation angle θ, as is shown by Equation 2.9.

The aligned electrodes thus ensure a uniform current distribution and electric field. Furthermore, aligned electrodes enable the use of Equations 2.10, 2.11, and 2.12; because $J_y = 0$. It is clear that when conducting resistivity/conductivity measurements on UD CFRP materials with off-axis fibre orientations, one should align electrodes with the fibre orientation.

3.4 Validation of 2D assumption

Up until this point, all phenomena described have been contained within the xy-plane. Out-of-plane effects have been neglected and assumed constant. The specimens represented in Figures 3.5-3.7, 3.9, and 3.10, have no thickness. However, in the following chapter, measurements are done on specimens with non-zero thicknesses. For this, the location of the terminal and ground become relevant in describing how current will flow through the material. Figure 3.11 illustrates how current would flow through a specimen with non-zero thickness. Here, guideline 4 of the measuring considerations becomes relevant.

As is outlined in the following chapter, all specimens tested have approximately the same thickness. To determine an appropriate D_{dev}, a 3D model is built with the appropriate specimen dimensions. The top and bottom voltage probes are fixed as a parametric sweep is carried out over D_{dev}. The difference in measured potential difference by the top and bottom probes is plotted in Figure 3.12. It can thus be concluded that a minimum distance of 10 [mm] must be assigned to D_{dev}. All materials tested in the following chapter have a relatively similar σ_3. Therefore, only one model needs to be made. Furthermore, the setup is symmetrical, so the horizontal distance between the terminal and the first electrode of either probe is the same as the

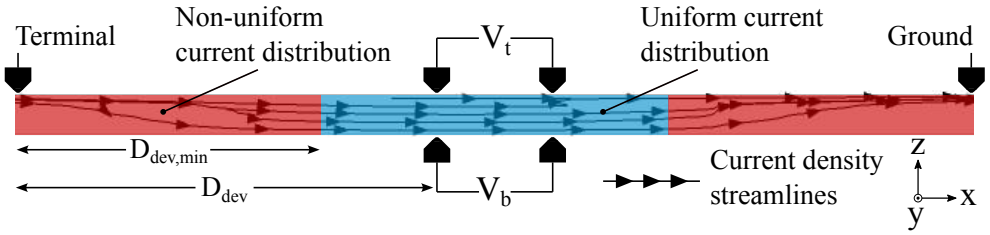

Figure 3.11: *Flow of current inside UD laminate viewed in the xz-plane.*

horizontal distance between the second electrode of either probe and the ground. Note that in this work, D_{dev} is not used to describe the minimum distance required for the current flow to be fully developed; it is the actual distance used in either the model or the experimental setup. Essentially, the D_{dev} used is larger than necessary. However, this does not take away from the fact that the 2D assumption is valid within this fully developed zone.

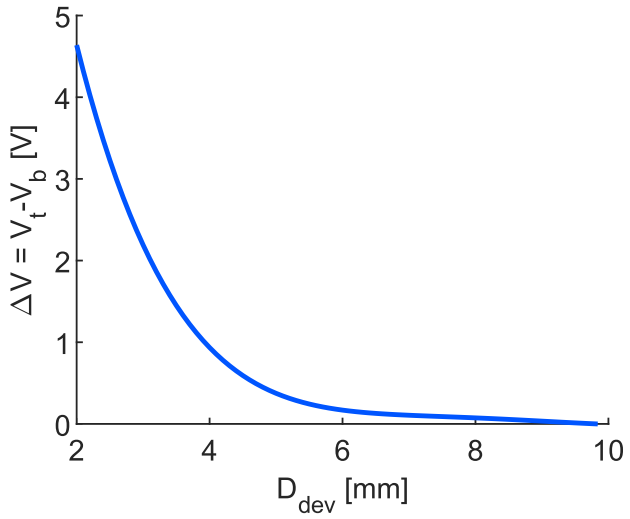

Figure 3.12: *Difference in simulated voltage between top and bottom probes for an 8-ply UD CFRP specimen.*

Now, the experimental setup can be built according to the model design. As long as the setup confines the voltage probes to the fully developed zone, the resulting measurement data can be compared to a 2D model.

Chapter 4

Experiments

This chapter presents the practical implementation of the six-probe method with aligned electrodes described in the previous chapter. The materials tested in this work are discussed along side the preparation of specimens. This is followed by a comprehensive overview of the measured data together with the employed analysis methods.

4.1 Material and specimen preparation

Laminates were prepared by stacking plies cut from 12 inch pre-impregnated rolls of composite tape. All stacks consist of eight UD plies. The stacked plies were consolidated in the press to form laminates. The edges of the consolidated laminates were trimmed and up to seven specimens were then cut out of each laminate using a CNC milling machine. This ensured a consistent width of 40 [mm] for all specimens. The thickness of each specimen was taken as the average of three measurements done with a digital micrometer at varying spots on the specimen. The average thickness of all specimens was approximately 1.11 [mm]; however, exact dimensions are taken into consideration during the analysis of the recorded data on every specimen. This is because the thickness and width of the specimens contribute to the calculated directional electrical properties, as was shown in Eqs. 2.10, 2.11, and 2.12.

Three materials were tested: Toray Cetex TC1200 AS4/PEEK [27], Solvay APC AS4D/PEKK [28], and Toray Cetex TC1225 T700G/LMPAEK [29]. All have a fibre volume fraction of $v_f = 0.59$. From each material, specimens were prepared with the following layups: $[30]_8$, $[45]_{4s}$, and $[60]_8$.

4.2 Experimental setup

With the aim of comparing collected data to simulated results, the experimental setup is made to closely resemble the models outlined in the previous chapter. Note that the model and setup change depending on the material and layup being tested. For example, the $\bar{\sigma}$ of the specific material being tested is used as input for the model. Similarly, When testing a $[45]_{4s}$ layup, the input variable θ must be adjusted accordingly.

Several important variables that are kept constant between each measurement of the same material and layup. In the case of the model, this can be done through a parametric sweep. In the case of the physical setup, the electrode aligning brackets, and the electrode clamps, serve as a repeatability assurance. The relevant variables are as follows:

- Vertical alignment of top probe and bottom probe
- Horizontal distance between first and second electrode of probes: δ_x
- Horizontal distance between terminal and first electrode of the probes: D_{dev}
- Alignment of electrode contacts with fibre orientation: θ

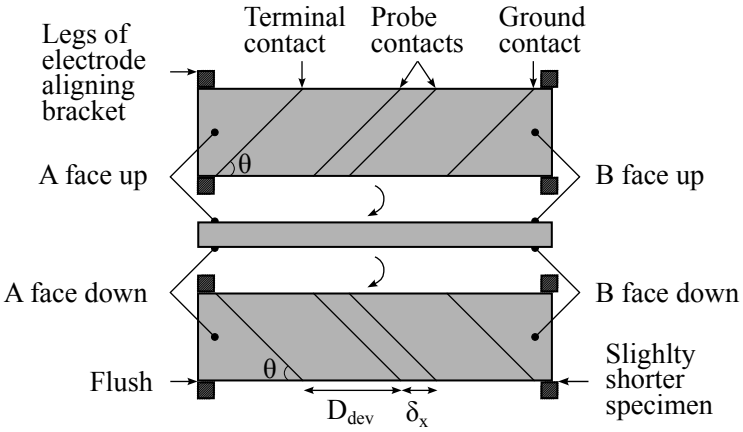

Figure 4.1: *Distinction between face up and face down of tested specimens.*

Each specimen is tested using the six-probe method to determine its electrical resistance. A direct current is introduced along a line contact on the top surface of the specimen at one end. On the top surface at the other end, a ground is applied, also along a line contact. Thereby resulting in current flowing inside the specimen. Four voltage probes are then used to measure a potential difference across the top and bottom surface of the specimen as shown in Figure 3.11. It is important to note that all probes are oriented such that they line up with the fibre orientation. This is to avoid the potential short circuits visualized in Figure 3.9.

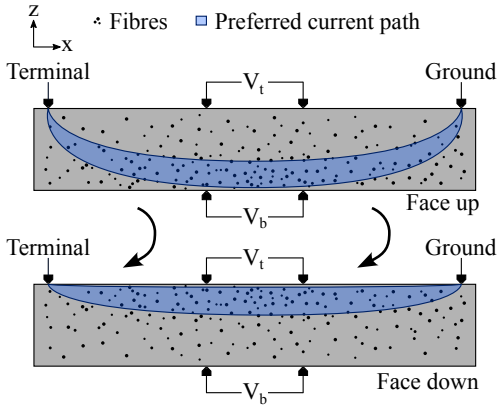

Figure 4.2: *Example of preferred current path inside a UD CFRP specimen caused by higher local fibre volume fraction.*

Furthermore, each specimen is tested face up and face down. The reason the specimen is tested twice is to account for inhomogeneities in the specimen. When observing the cross section of a laminate, one will find matrix rich regions as well as regions with relatively more fibre contact. Suppose the top of a specimen

has a matrix rich region and the bottom has a fibre rich region. Then, the current would be favored to flow through the bottom side as opposed to equally through the whole thickness. This would result in a higher current density near the bottom of the specimen. In Figure 3.11 this would be interpreted as more current density streamlines near the bottom relative to the top. The bottom probe would thus record a higher voltage, since the resistance is constant. Figure 4.2 clarifies this phenomenon. Flipping the specimen over gives insight into how homogeneous the specimen is. Additionally, the two measurements can be averaged to get rid of this uncertainty regarding homogeneity of the specimen.

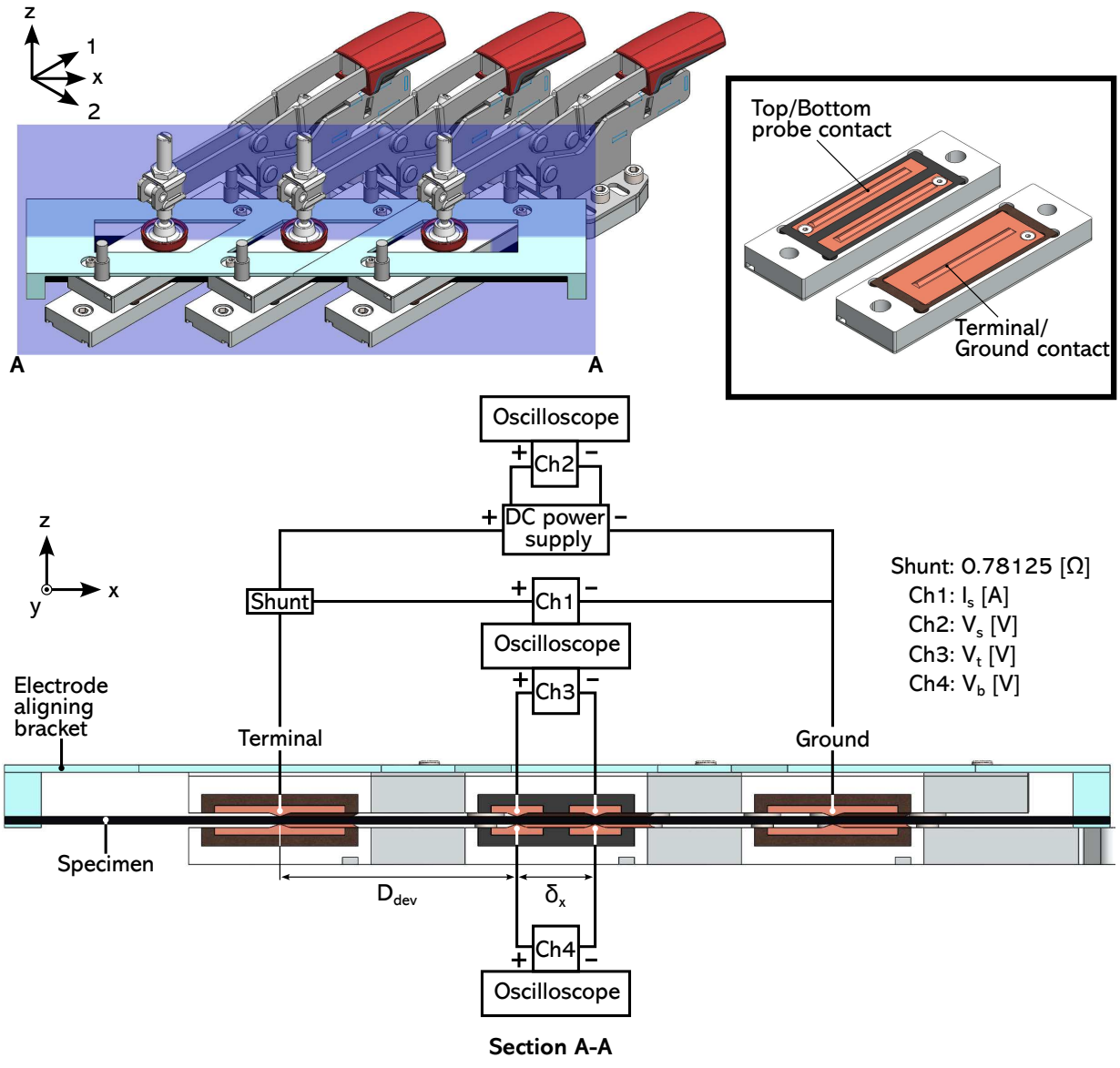

Figure 4.3: *Annotated illustration of the experimental setup used.*

To ensure that the same section of the specimen was tested in both measurements, the left side of the specimen was lined out flush with the electrode aligning bracket. This means that even if a specimen was

slightly longer or shorter than the bracket, the electrodes always made contact at roughly the same points. Figure 4.1 illustrates how each specimen was flipped over and aligned so as to keep contact points consistent. Note that when the specimen is flipped, the electrodes must undergo an in-plane rotation of 90° to align themselves with the fibres. Therefore, a total of two separate brackets per fibre orientation tested were printed. The brackets also serve to keep the electrodes parallel to each other. The whole setup for a 45°, face up, measurement can be seen in Figure 4.3.

Each specimen is tested through an applied voltage sweep ranging from 10 [V] to 60 [V]. This sweep is communicated to the power supply through a program written in MATLAB, making all runs consistent. An oscilloscope with three separate channels is used to record data saved as arrays in MATLAB. The different channels resulted in an array containing the current supplied by the power supply for a given voltage input, and the voltage difference on the top and bottom of the specimen. The current is measured by passing it through a current shunt with a known electrical resistance and measuring the voltage over the shunt. For each voltage step, the system is given the appropriate rise time to let the signal stabilize, after which samples are recorded with a sample frequency of 10 [kHz] for a total of 10,000 samples.

4.3 Results

A total of 15 laminates were press consolidated, out of which 56 specimens were prepared and tested. The measured voltage by the top probe (V_t) and bottom probe (V_b), together with the applied current is first used to determine the electrical resistance (R) of the specimen. This resistance is then substituted into Equations 2.10 and 2.11 to determine a ρ_{xx} and ρ_{xy} for each specimen. Furthermore, an apparent σ_2 is found for each specimen using Equation 2.12.

4.3.1 Press consolidation

The three materials were consolidated according to their respective press-cycle. This can be seen in Figure 4.4. In all cases, a heating rate of 10 [°C/min] and cooling rate of 5 [°C/min] is used.

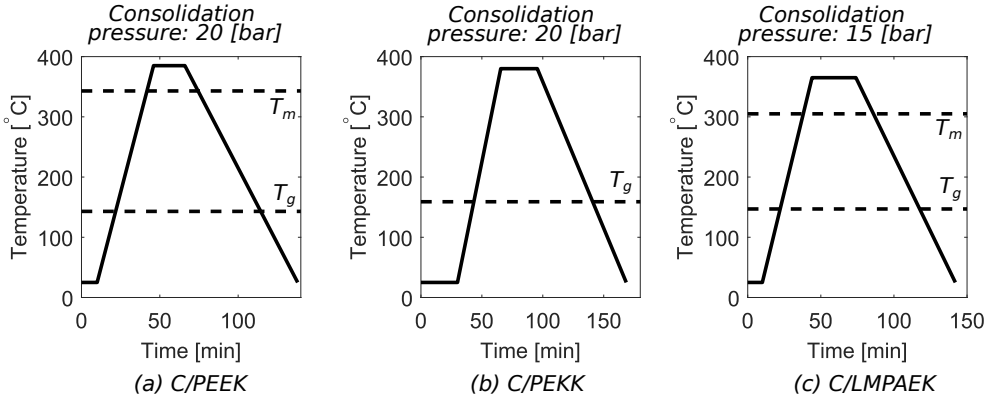

Figure 4.4: *Press consolidation cycles for the three different materials.*

Recovering fully intact laminates out of the press proved moderately challenging. Many of the laminates came out with cracks of varying sizes; some also had entire corners chipped off. From such laminates, little to no specimens could be prepared. In the case that parts of the laminate were usable, it was made sure that no cracks extended into the regions from which specimens were prepared. Nevertheless, excess laminates

were consolidated in an attempt to gather a minimum of four specimens per specimen type. The specimen type refers to the combination of material and fibre orientation of the specimen. An example of a chipped laminate is shown in Figure 4.5. This proneness to large crack formation is due to the unidirectional nature of the laminates. Note that the cracks form and propagate in the matrix material, not the fibres. For cross-ply laminates, for example, cracks are often stopped by fibres running transverse to the crack. However, in UD laminates, the cracks can more easily grow parallel to the fibres. This can also be observed in Figure 4.5. The break conforms to the fibre orientation inside the UD laminate.

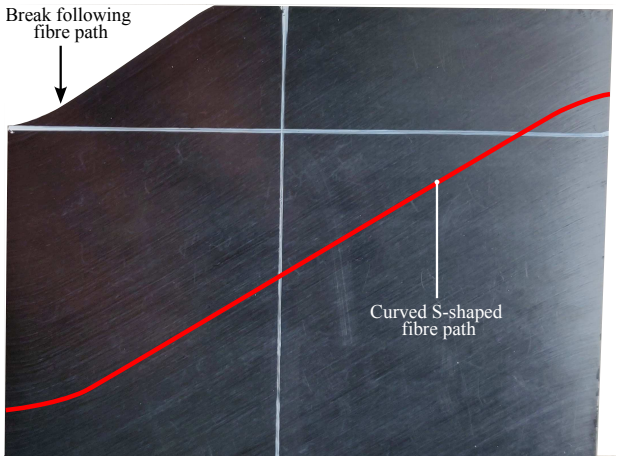

Figure 4.5: *Example of a curved fibre path found on the surface of a* $[30]_8$ *laminate.*

Furthermore, curved fibre paths were observed on the surface of several laminates. This occurrence was solely found on the 30° and 60° laminates; which are essentially the same laminate but rotated 90° in-plane. These curved fibre paths are an effect of the flow behaviour inside the mould during consolidation. This flow occurs because the laminate is slightly smaller than the mould. As the heated laminate is compressed, matrix material starts flowing towards empty spaces inside the mould. For UD laminates, flow is severely restricted transverse to the fibres. Matrix material thus flows along the fibres before transverse flow occurs. When the material comes in contact with the walls of the mould, the no-slip condition can be applied. This means that at the point of contact with the walls, the flow velocity is zero. Once longitudinal flow stops, the remaining empty space is filled by transverse flow. The UD fibres are displaced by the flow of matrix. However, this flow is subject to the no-slip condition at its edges. The flow can thus be split into two stages: initial longitudinal flow, followed by transverse flow. This, together with the no-slip condition at the walls of the mould explains why the fibres follow an S-shaped path as shown in Figure 4.5.

The reason that 45° laminates were less affected by this could be related to the aspect ratio of the mould. The mould is square, which has an aspect ratio of 1:1. 45° laminates share this aspect ratio, giving them a certain symmetry inside the mould. However, 30° and 60° laminates do not have this same symmetry. One way to validate this claim is to use a rectangular mould and laminate with matching aspect ratios. These aspect ratios are identical to the ones shown in Figure 3.2.

In the previous chapter it was shown that parallel fibres and electrodes are crucial for accurate measurements. The curved fibre paths observed after press consolidation are relevant because they introduce new short circuits which were not visualized in the previous chapter. Figure 4.6 illustrates how such a short circuit would look. The concept is the same as was discussed in the previous chapter. The current en-

counters significantly less electrical resistance along continuous fibres, making it a preferred path. This phenomenon occurs irrespective of the linearity of the fibre path.

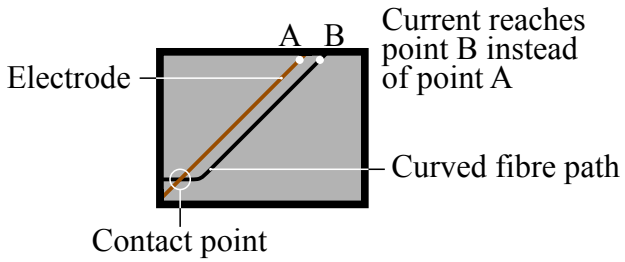

Figure 4.6: *Possible short circuit caused by curved fibre path during.*

The observed non-linear path of fibres thus needs to be considered before measurements can be done. The specimens originating from regions where this flow effect was not present could simply be used with no further requirements. The specimens in which the flow effect was present could also still be tested, as long as the flow effect did not extend into the zone in which the probes are placed. Figure 4.6 clarifies how this condition can be met.

4.3.2 Raw data

For each measurement done, four plots are generated. Note that a measurement refers to either face up or face down for a single specimen. These plots correspond to the data collected through the different oscilloscope channels. An example is include in Figure 4.7.

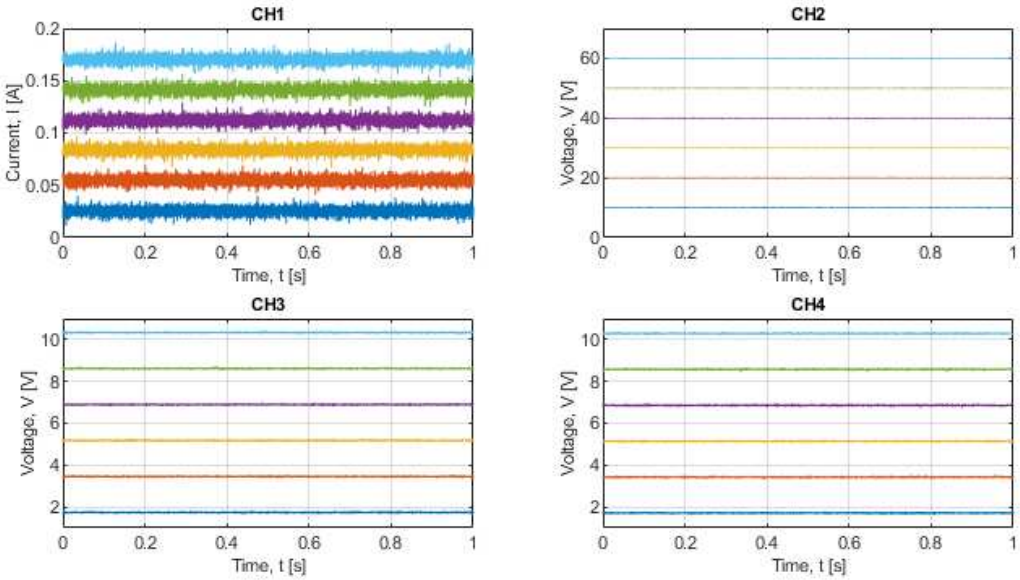

Figure 4.7: *Typical data set for a single measurement. Data from the four oscilloscope channels is plotted in MATLAB. See Figure 4.3.*

There is visible noise in the recorded current of channel 1. This is in part due to the range of the y-axis, and the equipment used. However, taking the average over this gives an acceptable approximation. Over-

all, this is a good measurement. The data is then used in the next analysis step to calculate the electrical resistance of the specimen.

4.3.3 Resistance

The recorded data at each voltage step is averaged before it is interpreted. For each specimen, the voltage difference measured by the top probe and bottom probe is plotted against the corresponding supplied current. This is done for both the face up and face down measurements, resulting in a V-I plot with four trends per specimen. As per Ohm's law, the gradient of the trend is the electrical resistance of the specimen. Essentially, there are four separate resistances which are obtained from each plot: $R_{u,t}$, $R_{u,b}$, $R_{d,t}$, $R_{d,b}$. Where the subscripts *u*, *d*, *t*, and *b*, stand for face up, face down, top probe, and bottom probe respectively. The average of the face down and face up measurements should lie relatively close to each other, because it is the same specimen being tested. Therefore, in the case that these averages lie too far apart, it can be said that the data for that specimen is unreliable. With this in mind, the V-I plot of a specimen can fall into one of three categories.

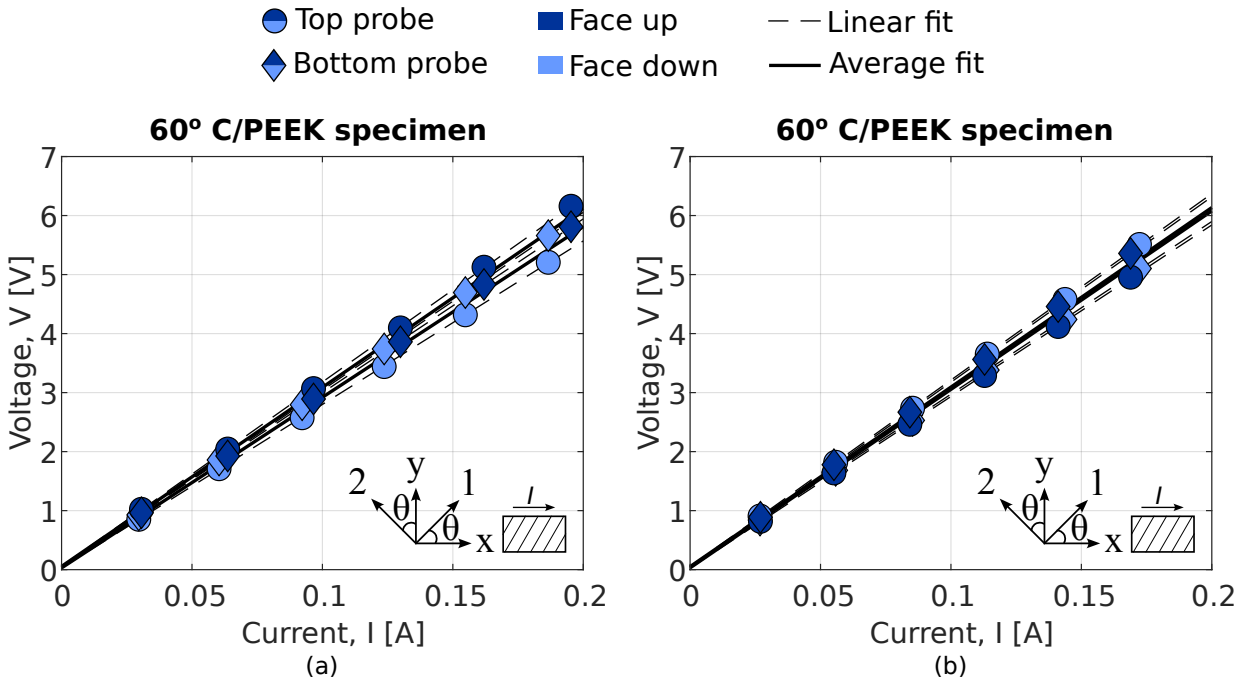

Figure 4.8: *Current and voltage data of (a) a 60° C/PEEK specimen, and (b) another 60° C/PEEK specimen. Both specimens have a preferred current path.*

The first category contains the non-homogeneous specimens. Generally, for a homogeneous specimen, the voltage measured by the top probe should be equal or slightly higher than that of the bottom probe. However, in practice, this is rarely the case. This category is the most common; containing approximately 75% of all specimens tested. Showcasing why it is beneficial to measure the specimen face up and face down. The indicative sign that a specimen is non-homogeneous can be seen in Figure 4.8. This is an example V-I plot of a non-homogeneous specimen. The face down measurement is the invert of the face up measurement. This means that there is a preferred current path within the specimen. This path can be more towards the top probe, or the bottom probe. An example of this was shown in Figure 4.2. This results in that probe measuring a higher voltage. Figure 4.8 (a) thus belongs to a specimen which has a preferred

current path near the top probe when face up. When the specimen is flipped over as shown in Figure 4.1, the preferred current path now lies near the bottom probe. The opposite is true for the specimen of Figure 4.8 (b). There, the preferred current path lies near the bottom probe when face up and near the top probe when face down. These preferred current paths are caused by the higher number of fibre to fibre contacts in those regions, allowing for more current flow. The contrast in local to global fibre volume fraction can be attributed to the manufacturing stage of the UD tapes, as well as the press consolidation stage of the UD laminates. As was previously discussed, UD laminates are especially prone to undesirable flow effects during press consolidation.

The second category contains homogeneous specimens. These generally result in a V-I plots where the top probe always measures a higher voltage, regardless of whether it is a face up or face down measurement. This can be seen in Figure 4.9 (b). Occasionally, some of these specimens also result in a face down measurement which is the invert of the face up measurement, as in the previous category. However, because the trends are so tightly grouped, the difference in measured voltage between the top and bottom probe is negligible. An example of this is shown in Figure 4.9 (a), where one can see that all four trends are tightly grouped.

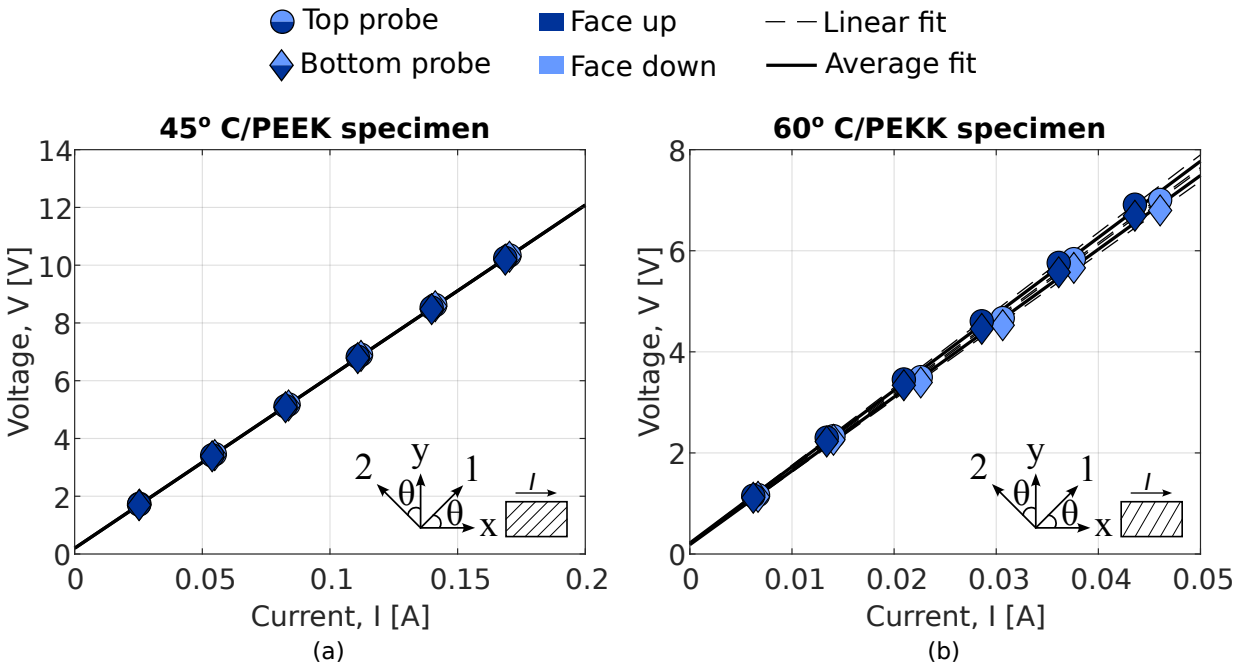

Figure 4.9: *Current and voltage data of (a) a 45° C/PEEK specimen, and (b) a 60° C/PEKK specimen. Both specimens are homogeneous, with no preferred current path.*

The last category contains specimens that show a significant difference between the face up and face down measurements. Technically, these specimens should fall into one of the previous two categories. However, the difference between the face up and face down measurements is significantly larger. Two examples are shown in Figure 4.10. In this work, the data collected on such specimens is deemed too inconsistent to be used for analysis. There are several issues which could be the cause of such deviation in the measurement results. One possibility is that one of the two measurements went well, while the other did not. For example due to poor or faulty electrical contact within the circuit. Most likely this would occur at a connection point from for example the shunt to the terminal. Similarly, both measurements could be of

poor quality. This uncertainty is what led to the decision to take data such as what is shown in Figure 4.10 out of the eventual data set.

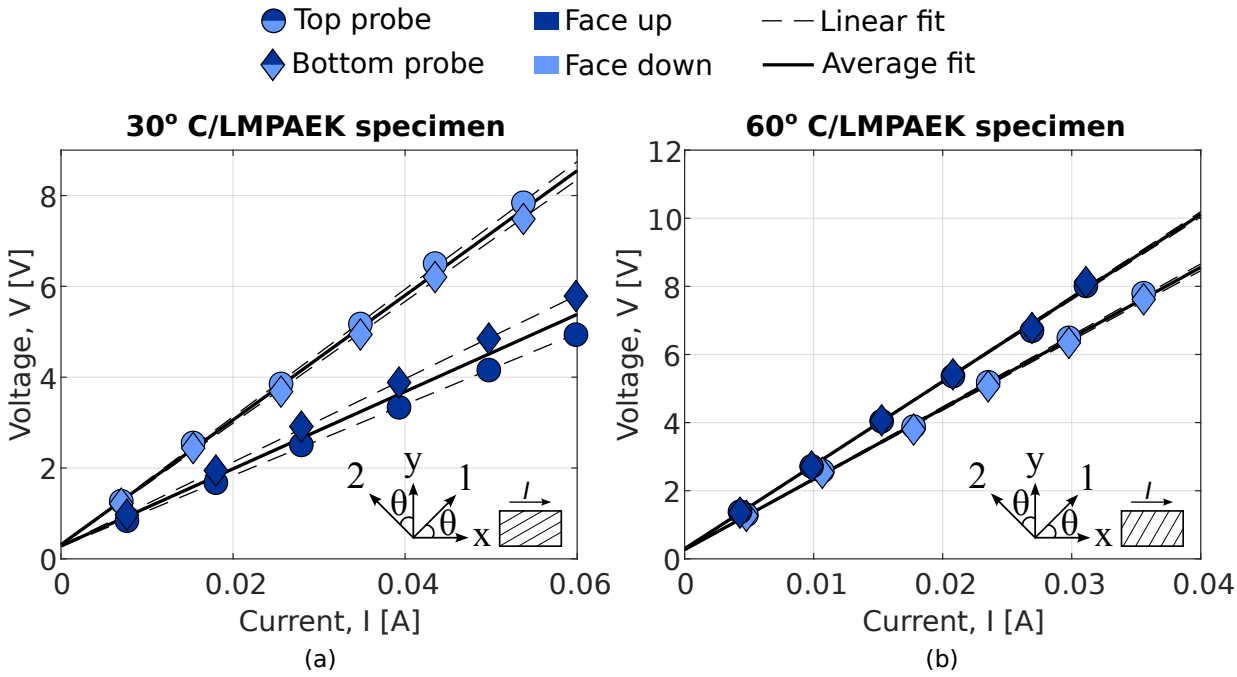

Figure 4.10: *Current and voltage data of (a) a 30° C/LMPAEK specimen, and (b) a 60° C/LMPAEK specimen. Both specimens show a large discrepancy between face up and face down measurements.*

Table 4.1: *Number of valid measurements (n_s) used for further analysis for each specimen type.*

θ	C/PEEK	C/PEKK	C/LMPAEK
30°	5	5	5
45°	7	7	6
60°	5	6	4

For all specimens, the average trend of the face up measurement was compared to the average trend of the matching face down measurement. If the absolute percentage error between these two trends is larger than 10%, the specimen is no longer considered for further analysis. For the specimens which have an error below this threshold, the average of all four trends is taken as the resistance for that specific specimen. This resistance is then used to determine the resistivity (ρ_{xx}) of each specimen. Table 4.1 gives an overview of the specimens considered for further analysis.

4.3.4 In-plane resistivity

The in-plane resistivity tensor was determined by calculating its components using Equations 2.10 and 2.11. Note that $A = wh$; where *w* [mm] is the width of the specimen, and *h* [mm] is its thickness. As was previously mentioned, the width of all specimens is assumed constant, while the thickness has small variations. Furthermore, δ_x depends on the fibre orientation, as discussed in the previous chapter. With this

in mind, the resistivities were calculated for each specimen, using the average resistance from the respective V-I plot. The average resistivities for the nine different specimen types tested are shown in Figure 4.11 together with the corresponding standard deviation as error bars. Only data from the specimens with a percentage error below 10% is included in Figure 4.11. Therefore, not all results are based on the same number of specimens. The number of specimens considered is denoted by an n_s value in the plot.

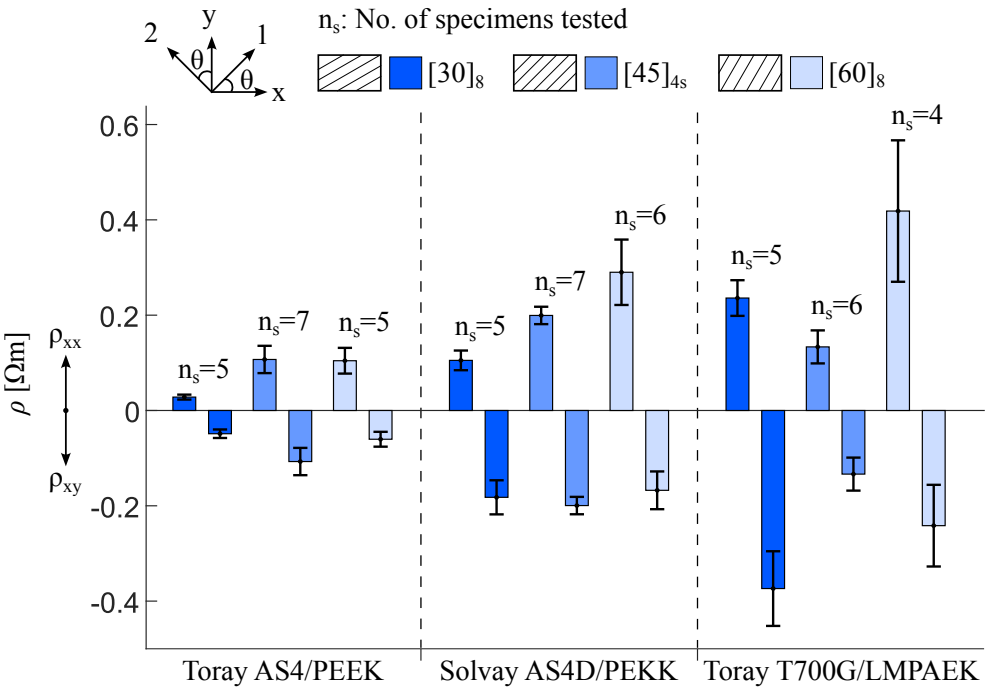

Figure 4.11: *Average ρ_{xx} and ρ_{xy} of UD CFRP specimens measured at varying fibre orientations.*

Even though the number of specimens that the results are based on differ per specimen type, Figure 4.11 still provides several insights. The first observation is that ρ_{xx} is always positive, while ρ_{xy} is always negative. This is a result of the manner in which the global coordinate system has been defined in this work. ρ_{xx} and ρ_{xy} depend on E_x and E_y respectively. It was shown in Figures 3.9 and 3.10 that for all three fibre orientations, the x-component of the electric field is always positive, while the y-component is always negative. The absolute value of the resistivity is of more interest; however, ρ_{xy} is kept negative to increase the readability of Figure 4.11.

When considering ρ_{xx}, one expects it to increase as the fibre angle increases. One can test this by substituting different values for θ into Equation 2.10, and keeping all other variables constant. This trend is clearly shown by the C/PEKK specimens. However, C/PEEK and C/LMPAEK specimens do not follow this trend. This unexpected behaviour could very well be a result of the low number of specimens tested. LMPAEK specimens also show the largest standard deviation. Because the data pool is relatively small, irregularities in the measurements or the specimens themselves have a much larger influence on the final result. Increasing the number of specimens tested could significantly increase the validity of the results.

When considering ρ_{xy}, one expects a certain symmetry. At 45°, it is at its highest. As θ increases and approaches 90°, it should decrease to 0 $[\Omega m]$. This trend should be mirrored when going from 45°down to 0°. Essentially, ρ_{xy} at 30°should be equal to ρ_{xy} at 60°. This can be tested through Equation 2.11. This trend

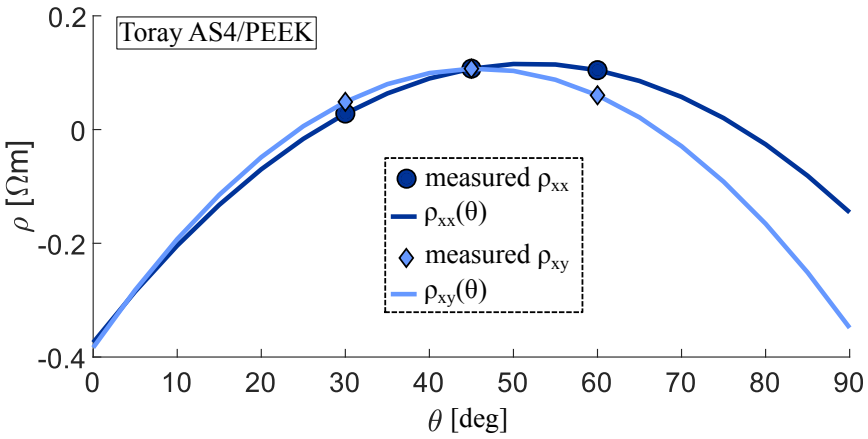

Figure 4.12: *ρ_{xx} and ρ_{xy} as functions of θ, based on measurement data from C/PEEK specimens.*

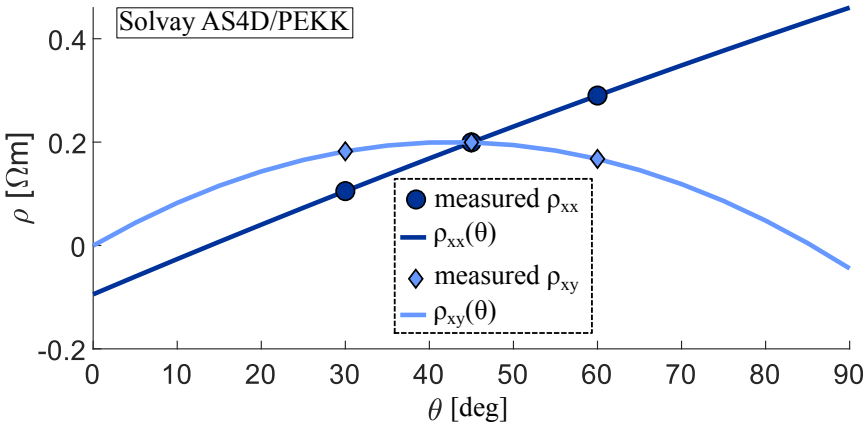

Figure 4.13: *ρ_{xx} and ρ_{xy} as functions of θ, based on measurement data from C/PEKK specimens.*

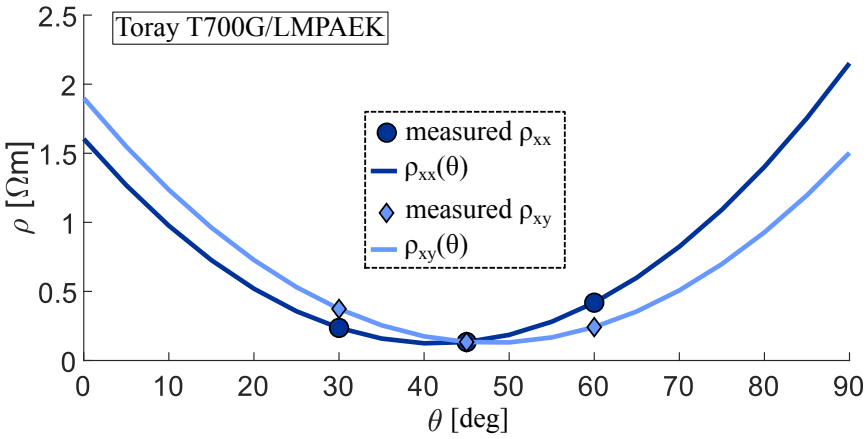

Figure 4.14: *ρ_{xx} and ρ_{xy} as functions of θ, based on measurement data from C/LMPAEK specimens.*

is visible for C/PEEK and C/PEKK specimens; however, the opposite is true for C/LMPAEK specimens. This is most likely also attributable to the relatively low number of specimens tested.

Using the data points for the three different fibre orientations shown in Figure 4.11, one can plot ρ_{xx} and ρ_{xy} as functions of θ. This is done by fitting a second order polynomial over the three data points. The results for C/PEEK, C/PEKK, and C/LMPAEK are shown in Figures 4.12, 4.13, and 4.14 respectively.

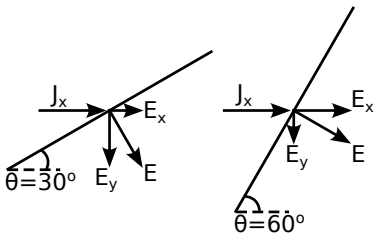

Figure 4.15: *Influence of fibre orientation on electric field components. Note the electric field always lies perpendicular to the equipotential lines, which correspond to the fibre orientation in this case.*

Comparing the absolute values of ρ_{xx} and ρ_{xy} to each other for each specimen type, one can notice a trend shared by all materials. Firstly, for $\theta = 45°$, $|\rho_{xx}| = |\rho_{xy}|$. This is because in the case of $\theta = 45°$, $\tan(\theta) = 1$. Moreover, when $\theta = 30°$, $|\rho_{xx}| < |\rho_{xy}|$; and when $\theta = 60°$, $|\rho_{xx}| > |\rho_{xy}|$. This is in line with the manner in which the electrical resistivity defines the electric field generated by a given current density. ρ_{xx} gives an indication of the magnitude of the electric field generated in the x-direction for a given current density in the x-direction. On the other hand, ρ_{xy} gives an indication of the magnitude of the electric field generated in the y-direction for a given current density in the x-direction. This means that if $|\rho_{xx}| > |\rho_{xy}|$, the generated electric field receives the largest contribution from its x-component. In the case that $|\rho_{xx}| < |\rho_{xy}|$, the generated electric field receives the largest contribution from its y-component. This is visualized in Figure 4.15. It is clear that at $\theta = 60°$, the x-component is larger than the y-component. The opposite is true at $\theta = 30°$.

Table 4.2: *Expected and average measured directional resistivities for off-axis UD CFRP specimens. Based on Figure 4.11, and Equations 2.10 and 2.11.*

Material	θ	Predicted ρ_{xx} $[\Omega m]$	Measured ρ_{xx} $[\Omega m]$	Error [%]	Predicted ρ_{xy} $[\Omega m]$	Measured ρ_{xy} $[\Omega m]$	Error [%]
C/PEEK	30°	0.037	0.028	-24	0.064	0.049	-24
	45°	0.074	0.107	45	0.074	0.107	45
	60°	0.111	0.105	6	0.064	0.060	6
C/PEKK	30°	0.070	0.105	50	0.121	0.182	50
	45°	0.140	0.200	42	0.140	0.120	42
	60°	0.210	0.290	38	0.121	0.168	38
C/LMPAEK	30°	0.073	0.236	226	0.126	0.374	198
	45°	0.145	0.134	-8	0.145	0.134	-8
	60°	0.217	0.417	93	0.126	0.242	92

The results have been summarised in Table 4.2. Overall, C/PEEK seems to have the lowest resistivity, while

C/PEKK and C/LMPAEK are slightly higher. The latter two are also quite comparable when it comes to resistivity. Here, one can also see the difference in expected resistivity and measured resistivity for all specimen types. Both resistivities are based on Equations 2.10 and 2.11. The expected resistivities are calculated using ρ_2. The ρ_1 term is neglected as it has an insignificant impact on the calculated value. The ρ_2 values used are taken from experimental work done by Buser [2]. The materials tested in that work are the same as in this work, except for the fact that different pre-preg rolls were used to prepare the laminates. The 8-ply UD specimens tested by Buser had a layup of $[0]_{4s}$; and a similar six-probe method was used specially for determining the in-plane transversal conductivity (σ_2). This σ_2 is then converted into ρ_2 to be used in this work.

4.3.5 In-plane transversal conductivity

Taking a step back to the average resistance interpreted from the V-I plots of the specimens, one can also calculate one of the three principal resistivities: ρ_2. This can be done using Equation 2.10. Because of the extremely high anisotropy of the material, this expression simplifies to Equation 2.12. Essentially, the fact that $\sigma_1 \gg \sigma_2$, and that ρ is the reciprocal of σ, results in $\rho_1 \ll \rho_2$. So much so, that the ρ_1 term barely contributes, and can therefore be taken out of the expression. Equation 2.12 thus makes it possible to determine a σ_2 for each specimen. The average σ_2 for the nine different specimen types tested are shown in Figure 4.16 together with the corresponding standard deviation as error bars. This is based on the same data set as Figure 4.11, which is described by Table 4.1. The collected data is compared to the results of the work done by Buser [2], also used for Table 4.2. It must be noted that that data is based on the average results for 15 specimens, which is a two to three fold increase is sample size when compared to this work.

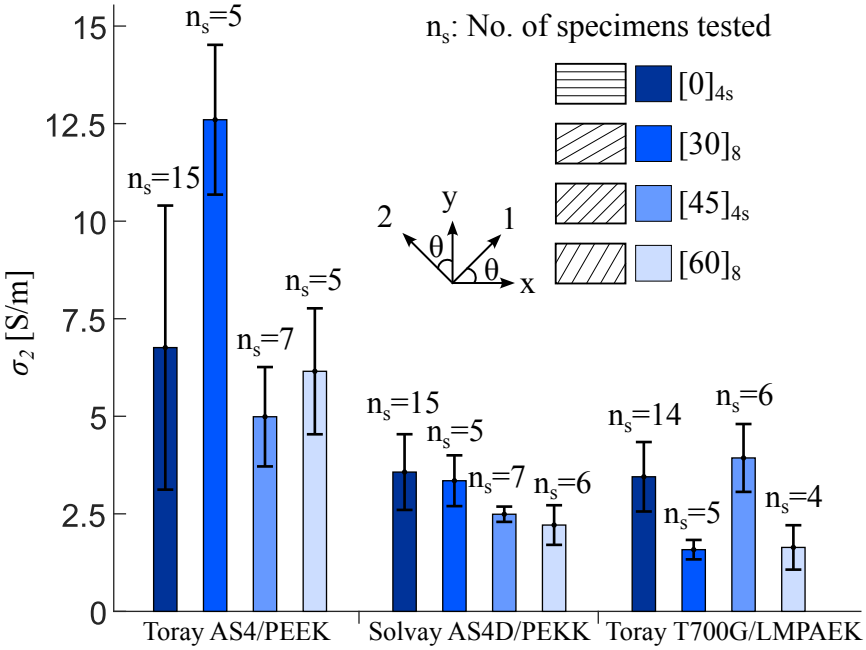

Figure 4.16: *Average σ_2 of UD CFRP specimens measured at varying fibre orientations. The data for the $[0]_{4s}$ specimens was taken from [2].*

The collected data shows some spread in the calculated σ_2. For a single material, one expects a consistent σ_2, regardless of the fibre orientation. However, this is not entirely the case when looking at Figure 4.16. C/PEKK specimens have the least amount of spread. Furthermore, when considering the standard

deviations, one can see that these also lie close to each other. On the other hand, C/PEEK and C/LMPAEK specimens have a larger spread. Still, when comparing the result of this work to the result of the work done by Buser [2], the possible values for σ_2 are relatively close together. When comparing the materials, it is clear that C/PEEK specimens have the highest in-plane transversal conductivity. This could also be observed in Figure 4.11, where C/PEEK specimens showed the lowest resistivities.

When looking at the C/PEKK data, one might observe that as the fibre angle increases, the average measured σ_2 decreases. This would mean that either measuring at large fibre angles underestimates the value of σ_2, or measuring at small fibre angles overestimates σ_2. However, this is inconclusive. Because this trend cannot be seen in the C/PEEK or C/LMPAEK data.

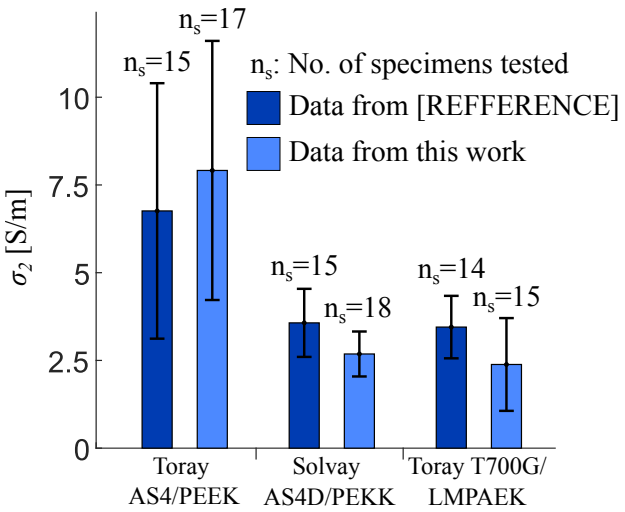

Figure 4.17: *Average σ_2 based on all fibre orientations tested in this work, compared to the results from [2].*

Since the measured σ_2 should be the same, regardless of the fibre orientation, the data was combined for each material. As can be seen in Figure 4.17, the results are in good agreement with those found by Buser [2].

Chapter 5

Discussion & Recommendations

Four measuring considerations were introduced in Chapter 2 to serve as guidelines for conducting electrical conductivity/resistivity measurements. A measurement method was designed with the aim of measuring the off-axis electrical resistivity (ρ_{xx}) of UD CFRP laminates. To this end, six electrodes are used, with one top probe and one bottom probe. Line contacts are used, and these are aligned with the fibre orientation to avoid short circuits. Furthermore, the aspect ratio of the specimens is chosen such that there are no continuous fibre paths between terminal and ground and there is sufficient distance between the terminal and probes for current to fully develop. The results are compared to an expected value calculated using analytical expressions. While considerable error is found, the measured data in this work is in line with the results found by Buser [2] in another study.

5.1 Method results

As was shown in Table 4.2, there is a significant discrepancy between the off-axis resistivity predicted with the analytical expression and the one calculated using the measurement data. The error is not consistent between different fibre angles or between different materials. However, for seven out of the nine specimen types, the measured ρ_{xx} and ρ_{xy} values underestimate the predicted ones.

This can be interpreted in two distinct ways. Either the analytical expressions are not sufficiently complex to determine the off-axis resistivity of UD laminates, or the measurements are invalid. In case of the former, there are potentially contributions which have not been considered and result in missing terms in the analytical expressions. On the other hand, one could argue that the measurements are not ideal, and thus error should always be expected. While this is true, the inconsistency of the error, as well as its magnitude indicates that there is still more to be understood about off-axis resistivity of UD laminates.

Even though the error is significant, the results found in this work are still in line with the results found in another study. This is a good sign for validity of the measurement method. Looking at the results, it is clear that for now the measurement method is needed to determine the off axis resistivity of UD laminates. Simply knowing σ_1 and σ_2, and using the analytical expressions is not sufficient. Before the employed measuring method can be recommended, its reliability and validity must be discussed.

5.2 Method reliability

One way to assess the reliability of the developed test method is to consider the repeatability of the measured data. As was shown by Figure 4.17, there is still a considerable amount of spread in the measured σ_2. While C/PEKK has the lowest standard deviation, at around 24% of the average. The standard deviation for C/PEEK and C/LMPAEK is 47% and 55% of the average, respectively. Even though this is quite significant. It could in large part be caused by the material itself.

When it comes to CFRP's, there are a number of reasons why inconsistent measurements can be attributed to the material. It is well documented that the material structure, or morphology, of composite tapes can vary drastically between manufacturers. Furthermore, tapes cut from rolls belonging to different batches can also have distinct structures, even if they are produced in the same manufacturing facility. The batch number of a roll says something about the date of manufacturing. It is thus important to consider this when working with CFRP materials. This is not an issue for electrical properties in the 1-direction. Essentially, all three conductivities depend on the fibre conductivity (σ_f). The difference being that the conductivity in the 2- and 3-direction are sensitive to the morphology and depend on fibre-to-fibre contacts. In Figure 4.2 it was shown how this can result in the formation of preferred current paths. The C/PEKK specimens are the only ones which all originated from the same roll in this work. In the case of C/PEEK and C/LMPAEK, the specimens were made from two separate rolls. This might be a reason that the spread in measured σ_2 is lower for C/PEKK.

Furthermore, the data from this work, shown in Figure 4.17, is based on specimens taken out of different laminates. This adds more chance for variations to occur, because the consolidation itself can affect the final architecture of the fibres, especially for fully unidirectional lay-ups. Attempts are made to ensure as much consistency as possible. For example using the same process settings for the press consolidation stage. These settings were kept constant based on the material. However, one could argue that a better method would be to cut all specimens from the same laminate. This could be done by press consolidating a $[0]_{4s}$ laminate and using a CNC to cut out specimens with varying fibre orientations. Figure 5.1 illustrates how this would look. The disadvantage of this is that the specimens would have to be made significantly smaller if the same number of specimens need to be cut out of a single laminate. One would still have to ensure an aspect ratio larger than the critical aspect ratio for the given fibre orientation. A new physical setup would have to be made to allow the testing of these smaller specimens. Using point-contact electrodes could also prove useful in this case. Specimens that keep a constant length but have a smaller width also have a higher resistance, meaning that less current will pass through for the same voltage applied. Depending on the accuracy of the measuring equipment used, such low currents might not be feasible.

5.3 Method validity

The validity of the measurements is another metric that can be used to determine the quality of the data gathered using the developed method. It was shown in Table 4.2 that there is a large discrepancy between the measured ρ_{xx} and the predicted ρ_{xx}. While the absolute difference seems small, the percent difference is significant. This is especially an issue for the C/LMPAEK measurements. One might argue that theoretical conditions could never be met. So in practice for example the fibres are not all oriented at θ exactly. It is true that this could influence the measurement. However, that would not result in an average difference of over 50% between predicted and measured.

Another argument could be that a much larger number of specimens need to be tested to reduce the effect

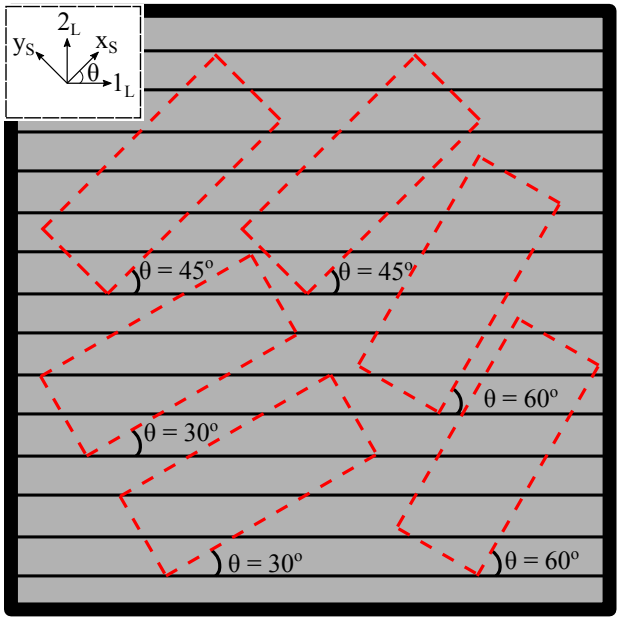

Figure 5.1: *Sketch of potential CNC program to produce specimens with varying fibre orientations out of a single laminate. The subscripts L and S refer to the laminate and specimen coordinate system respectively.*

of measurement inconsistencies. While this is simple to do, it would most likely require that specimens are made from multiple different laminates, which could bring in more variation to the data.

Lastly, the large error could be attributed to the sensitivity of the measuring equipment itself. The currents achieved during experiments did not exceed 1 [A]. An indicative range of currents can be found in Figures 4.8-4.10. The equipment used is intended for currents as low as 0.1 [A] according to the manufacturer. Some measurements did not reach this threshold. To increase the current, thicker and/or wider specimens should be used.

For wider specimens, the idea of cutting all specimens out of a single laminate becomes even less plausible. So thicker laminates seems like the better option. One must consider that with thicker laminates, the minimum distance between the terminal and first electrode of the probe (D_{dev}) will also increase (see Figure 3.11). Thicker specimens can also introduce new uncertainties regarding out-of-plane conductivity. This was not considered in this work. However, as was illustrated in Figure 3.11, current also flows in the z-direction. Electrical conductivity in this direction is dominated by σ_3. Unlike σ_2, σ_3 also considers current flow between layers. There is a contact resistance between the adjacent plies which is different to that between adjacent fibres. As one can imagine, the effect of this contact resistance increases as the number of layers increase. A portion of the resistivity measured in the x-direction thus originates from a current flowing in the z-direction. For thin specimens, this can be neglected. However, with thicker specimens, this contribution could become more significant.

Chapter 6

Conclusion

To better understand to electrical behaviour inside complex fibre networks, varying current and voltage distributions inside UD CFRP materials have been visualised using numerical modelling. The insights gained can be used as guidelines during the measuring of electrical properties of UD CFRP materials. This led to the development of a measurement method for UD CFRP materials with off-axis fibre orientations that can be used to measure directional resistivities/conductivities.

The use of a six-probe method is advisable, as it allows one to account for material inhomogeneities. Measuring each specimen twice by flipping it over is also a good way to improve the validity of the data. When using line-contact electrodes, it is essential to align these with the fibre orientation. It has been shown that unwanted short circuits can occur otherwise. If, instead, point-contact electrodes are used, these must be aligned in the test direction (x-direction in this work). Regarding the geometry of the specimens; one must ensure that no continuous fibres provide a direct path between the terminal and ground electrodes. Therefore, an aspect ratio larger than the critical aspect ratio must be used for all specimens. Furthermore, specimens must be long enough to allow the current flow to fully develop. The voltage probes should also be placed within the fully developed (uniform current distribution) zone. This means that the distance between the terminal and first electrode of the probe (D_{dev}) must be long enough. Specimens should also be inspected to ensure there are no curved fibre paths within the measurement zone. These curved fibre paths can form during the press consolidation step and are mostly found near the edges of the consolidated laminate.

The developed method was used to collect data on three highly relevant materials in the aerospace industry with three different fibre orientations. The results show considerable spread. However, it must be noted that they are in good agreement with data from other authors. The spread in results could be attributed to the large variation in material morphology which can be found when working with CFRP materials. The argument being that inconsistent material structure results in inconsistent measurement data. This is especially relevant for the electrical properties transverse to the fibre direction, which are in large part governed by the fibre volume fraction.

From the data gathered in this work, it can be concluded that physical testing is still required for determining the off-axis resistivity of UD CFRP laminates. Simply knowing the principal, in-plane, resistivities (ρ_1 and ρ_2) is not sufficient. Further research needs to be done with the aim of reducing the error between measured and predicted off-axis resistivity. This will enable accurate models capable of predicting the directional resistivity regardless of fibre orientation.

Bibliography

[1] S. Prashanth, S. Km, N. K, and S. S, "Fiber reinforced composites -a review," *J Material Sci Eng*, vol. 6, p. 341, 2017. (page 1)

[2] Y. Buser, "Internal report tprc." (page 2, 3, 4, 7, 39, 40, 41)

[3] S. Kesarwani, "Polymer composites in aviation sector a brief review article," *International Journal of Engineering Research Technology (IJERT)*, 2017. (page 1)

[4] G. Gardiner, "Welding thermoplastic composites." https://www.compositesworld.com/articles/welding-thermoplastic-composites, 2018. (page 2)

[5] A. P. da Costa, E. C. Botelho, M. L. Costa, N. E. Narita, and J. R. Tarpani, "A review of welding technologies for thermoplastic composites in aerospace applications," *Journal of Aerospace Technology and Management*, vol. 4, pp. 255–265, 2012. (page 2)

[6] T. J. Ahmed, D. Stavrov, H. E. Bersee, and A. Beukers, "Induction welding of thermoplastic composites—an overview," *Composites Part A: Applied Science and Manufacturing*, vol. 37, pp. 1638–1651, 10 2006. (page 3)

[7] M. Dhondt, "Induction welding of high performance thermoplastic composites: Focused heat generation in weld zones of carbon fiber laminates by magnetic field manipulation and carbon fiber susceptors," 2019.

[8] M. Holland, M. J. van Tooren, D. Barazanchy, and J. Pandher, "Modeling of induction heating of thermoplastic composites," *https://doi.org/10.1177/0892705720911979*, vol. 35, pp. 1772–1789, 4 2020.

[9] J. P. Reis, M. de Moura, and S. Samborski, "Thermoplastic composites and their promising applications in joining and repair composites structures: A review," *Materials 2020, Vol. 13, Page 5832*, vol. 13, p. 5832, 12 2020.

[10] P. G. O'Shaughnessey, M. Dubé, and I. F. Villegas, "Modeling and experimental investigation of induction welding of thermoplastic composites and comparison with other welding processes," *http://dx.doi.org/10.1177/0021998315614991*, vol. 50, pp. 2895–2910, 1 2016.

[11] A. Patel, M. Ali, and M. van Tooren, "Modelling of induction heating of thermoplastic composites using microscopic level modeling," *AIAA Scitech 2020 Forum*, vol. 1 PartF, 2020.

[12] T. Bayerl, M. Duhovic, P. Mitschang, and D. Bhattacharyya, "The heating of polymer composites by electromagnetic induction – a review," *Composites Part A: Applied Science and Manufacturing*, vol. 57, pp. 27–40, 2 2014. (page 3)

[13] N. Athanasopoulos and V. Kostopoulos, "Prediction and experimental validation of the electrical conductivity of dry carbon fiber unidirectional layers," *Composites Part B: Engineering*, vol. 42, pp. 1578–1587, 9 2011. (page 8, 9, 10, 12)

[14] J. H. Greenwood, S. Lebedat, and J. Bernasconit, "The anisotropic electrical resistivity of a carbon fibre reinforced plastic disc and its use as a transducer," *Journal of Physics E: Scientific Instruments*, 1975.

[15] A. S. Kaddour, F. A. Al-Salehi, S. T. Al-Hassani, and M. J. Hinton, "Electrical resistance measurement technique for detecting failure in cfrp materials at high strain rates," *Composites Science and Technology*, vol. 51, pp. 377–385, 1 1994.

[16] R. H. Knibbs and J. B. Morris, "The effects of fibre orientation on the physical properties of composites," *Composites*, vol. 5, pp. 209–218, 9 1974.

[17] K. W. Tse, C. A. Moyer, and S. Arajs, "Electrical conductivity of graphite fiber-epoxy resin composites," *Materials Science and Engineering*, vol. 49, pp. 41–46, 6 1981.

[18] M. Weber and M. R. Kamal, "Estimation of the volume resistivity of electrically conductive composites," *Polymer Composites*, vol. 18, pp. 711–725, 1997. (page 8, 12)

[19] N. Athanasopoulos, D. Sikoutris, N. J. Siakavellas, and V. Kostopoulos, "Electrical resistivity prediction of dry carbon fiber media as a function of thickness and fiber volume fraction combining empirical and analytical formulas," *Composites Part B: Engineering*, vol. 81, pp. 26–34, 11 2015. (page 9, 10)

[20] J. B. Park, T. K. Hwang, H. G. Kim, and Y. D. Doh, "Smart materials and structures experimental and numerical study of the electrical anisotropy in unidirectional carbon-fiber-reinforced polymer composites," *Smart Mater. Struct*, vol. 16, pp. 57–66, 2007. (page 9, 10, 11)

[21] R. Schueler, S. P. Joshi, and K. Schulte, "Conductivity of cfrp as a tool for health and usage monitoring," 1997. (page 10)

[22] N. Athanasopoulos and V. Kostopoulos, "Resistive heating of multidirectional and unidirectional dry carbon fibre preforms," *Composites Science and Technology*, vol. 72, pp. 1273–1282, 6 2012. (page 10, 11, 25)

[23] N. Athanasopoulos and V. Kostopoulos, "A comprehensive study on the equivalent electrical conductivity tensor validity for thin multidirectional carbon fibre reinforced plastics," *Composites Part B: Engineering*, vol. 67, pp. 244–255, 12 2014. (page 10, 11, 25)

[24] W. J. Grouve, F. Sacchetti, E. J. Vruggink, and R. Akkerman, "Simulating the induction heating of cross-ply c/pekk laminates – sensitivity and effect of material variability," *https://doi.org/10.1080/09243046.2020.1783078*, pp. 1–22, 2020. (page 10)

[25] Y. Buser, G. Bieleman, W. Grouve, S. Wijskamp, and R. Akkerman, "Characterisation of orthotropic electrical conductivity of unidirectional c/paek thermoplastic composites," 2022. (page 10)

[26] R. Schueler, S. P. Joshi, and K. Schulte, "Damage detection in cfrp by electrical conductivity mapping," *Composites Science and Technology*, vol. 61, pp. 921–930, 5 2001. (page 11, 25)

[27] "Toray cetex ® tc1200 peek product data sheet." https://www.toraytac.com/product-explorer/products/ovl4/Toray-Cetex-TC1200, 2019. (page 27)

[28] "Solvay apc (pekk)/as4d product data." https://www.solvay.com/en/product/apc-pekkas4d#product-documents. (page 27)

[29] "Toray cetex ® tc1225 lmpaek product data sheet." https://www.toraytac.com/product-explorer/products/gXuK/Toray-Cetex-TC1225, 2023. (page 27)